Escola de Camins
Escola Tècnica Superior d'Enginyeria de Camins, Canals i Ports
UPC BARCELONATECH

TREBALL FINAL DE GRAU

Feasibility of coal combustion by-products inertization for carbon capture and storage: the case for high-Ca fly ashes.

Treball realitzat per:
Jordi Soldevila Motta

Dirigit per:
Ignasi Casanova Hormaechea

Grau en:
Enginyeria Geològica

Barcelona, 26/01/2018

Departament de Enginyeria civil i ambiental

Acknowledgements

I would like to express my very great appreciation to Dr. Ignasi Casanova who introduced me to geoengineering of CO_2 storage technologies and mentored me throughout this thesis development.

I would like to offer my special thanks to Agnieszka Ćwik and Kwon Rodriguez who helped me with the experimental procedures, results interpretation and thesis assessing.

I am particularly grateful for the assistance given by Dr. Michela Romanini, who helped me operate the XRD equipment and was very supportive towards laboratory practical issues, and Dr. Trifon Todorov, who help to operate the SEM equipment and was very supportive towards laboratory practical issues.

I am grateful to the UPC (Universitat Politècnica de Catalunya) and UB (Universitat de Barcelona) for all this years of education.

Finally, I would like to offer my special thanks to my family who have always been next to me and have always been encouraging to study.

Abstract

The increase of carbon dioxide in the atmosphere is attributed to anthropogenic activities, mainly to the combustion of fossil fuels. In this regard, carbon capture and storage (CCS) technology is viewed as the main low-carbon technology, which can accomplish the objective, proposed in the Paris summit 2015, of limiting the global warming to no more than 2ºC. Fly ash can be enhanced to develop a significant technique to safely store carbon dioxide. The main purpose of this thesis was to demonstrate the feasibility to use coal combustion fly ash to sequester CO_2 under mineral form, mainly via CaO carbonation. Direct mineral (dry and wet) carbonation of coal fly ash from two different power plants (Andorra and Ptolemais) were studied under varying temperature (160ºC-220ºC) and constant CO_2 partial pressure (1 bar) conditions. On completion of the experiment, most of the samples had an increase in the carbonates proportion and it was clearly determined by using the following methods: powder XRD and Scanning electron mapping (SEM). However, XRD results revealed that only high calcium fly ash had calcium carbonate formation. SEM reveals clearly the changes caused by carbonation reaction by showing the formation of isolated calcite and needle-shaped structures, which could correspond to Aragonite, and coating on the surface of cenospheres. The fly ashes samples showed a clear carbonation trend. The Ptolemais fly ash sample (PT/3) that was under wet conditions and a temperature of 160º was the sample that presented the highest carbonation rate.

Resumen

El aumento del dióxido de carbono en la atmósfera se atribuye principalmente a la combustión de combustibles fósiles. En este sentido, la tecnología de captura y almacenamiento de carbono (CCS) se considera la principal tecnología baja en carbono que puede lograr el objetivo, propuesto en la cumbre de París de 2015, de limitar el calentamiento global a no más de 2ºC. La ceniza volante se puede acelerar para que de esta manera se pueda desarrollar una técnica significativa para el almacenamiento seguro de dióxido de carbono. El objetivo principal de esta tesis fue demostrar la viabilidad de utilizar cenizas volantes de combustión de carbón para secuestrar CO_2 en forma mineral principalmente a través de la carbonatación CaO. Se estudió la carbonatación mineral directa (seca y húmeda) de las cenizas volantes de carbón de dos centrales eléctricas diferentes (Andorra y Ptolemais) bajo diferentes condiciones de temperatura (160ºC-220ºC) y presión constante de CO_2 parcial (1 bar). Al finalizar el experimento, la mayoría de las muestras tuvieron un aumento en la proporción de carbonatos y se determinó claramente mediante el uso de los siguientes métodos: DRX en polvo y mapeo electrónico de barrido (SEM). Los resultados de XRD revelan que solo las cenizas volantes con un alto contenido de calcio han formado carbonato de calcio. SEM revela claramente los cambios causados por la reacción de carbonatación al mostrar la formación de cristales aislados de calcita y estructuras en forma de aguja, que podrían corresponder a aragonito, y el recubrimiento de la superficie de las cenoesferas. Las muestras de cenizas volantes muestran una clara tendencia a la carbonatación. La muestra de cenizas volantes de Ptolemais (PT / 3) que se encontraba bajo condiciones húmedas y a una temperatura de 160º fue la muestra que presento la tasa de carbonatación más elevada.

Keywords

IPCC Intergovernmental Panel on Climate Change
GHG Greenhouse Gases
RF Radiative Forcing
CCS Carbon Capture and Storage
CCP Carbon Combustion Products
IEA International Energy Agency
ACAA American Coal Ash Association
HCFA High Calcium Fly Ash
ASR Alkali-Silica Reaction
CCP Coal combustion product
AMC Accelerated Mineral Carbonation
XRD X-Ray Diffraction
FTIR Fourier-Transform Infra-Red
SEM Scanning Electron Microscopy
nm nanometer
SED Secondary Electron Detector
EDS Energy Dispersive Spectroscopy
BSD BackScattering Detector
CFA Coal fly ash

Table of Contents

List of figures

List of tables

1 State of the Art

1.1 Corroboration of Climate change

The Intergovernmental Panel on Climate change (IPCC) has established that the increase of greenhouse gases to the atmosphere and global warming are related. Human influence on global warming is clear and the recent emissions of greenhouse gases produced by anthropogenic activities have reached the highest concentrations in the history. The warming of the climate system is unequivocal and recent changes have been observed such as an increase of surface and sea temperature (0.167ºC since 1969); shrinkage of snow and ice sheets such as Antarctica (about 152 cubic kilometres diminished between 2002 and 2005) and Greenland (between 150 and 250 cubic kilometres diminished between 2002 and 2006) and the sea level has risen about 16 inches during the last 20 years. (IPCC, 2014). Anthropogenic emissions have increased the concentration of GHG, mainly carbon dioxide, since the pre-industrial era, driven by the economic and demographic growth. This has led to an increase of these gases only comparable at least to the last 800000 years and potentially the last 3 to 20 million years. The largest source of GHG gases from the anthropogenic activities is the burning of fossil fuels for electricity, heat and transportation. These activities have raised atmospheric carbon dioxide levels from 280 parts per million to 400 parts per million in the last 150 years.

Table 1.Anthropogenic sources of carbon dioxide. (IPCC,2005)

Process	Number of sources	Emissions ($MtCO_2\ yr^{-1}$)
Fossil fuels		
Power	4,942	10,539
Cement production	1,175	932
Refineries	638	798
Iron and steel industry	269	646
Petrochemical industry	470	379
Oil and gas processing	Not available	50
Other sources	90	33
Biomass		
Bioethanol and bioenergy	303	91
Total	7,887	13,466

The increment of the total cumulative atmospheric CO_2 concentrations due to anthropogenic emissions has resulted in the oceans absorbing at a rate of 7 Gt/year causing a decrease in the pH of the upper layers of 0.1. (IPCC, 2014). The ocean is the main reservoir of carbon (40000 Gt) and it plays a significant role in the study of atmospheric carbon dioxide. Other important reservoirs of carbon are the biosphere, soil and atmosphere. The oceanic and terrestrial CO_2 reservoirs have continued to absorb more than half of the total emissions of CO_2.However, these natural sinks of carbon dioxide will decrease in efficiency during this century and the terrestrial sink could even start to emit carbon dioxide. (Ronald et al., 2002, Friedlingstein et al. 2006). As a result, a long-term decrease would enhance climate change via an increase in the amount of carbon dioxide remaining in the atmosphere. (Copenhagen diagnosis)

Table 2. Approximate distribution of carbon in nature relative to the atmospheric carbon dioxide. (Ronald et al., 2002)

Source	Relative amount of carbon
CO_2 in the atmosphere	1
Total dissolved inorganic carbon	49.5
As H_2CO_3	0.3
As HCO_3^-	44
As CO_2^{3-}	5
Dissolved organic carbon	1.3
Particulate organic carbon	0.04
Terrestrial plants	0.56–1.1
Carbon in soils	1.6–2.1
Estimate of recoverable fossil fuels	5.3
Organic sediments	13,000
Inorganic sediments (carbonates)	65,000

Total anthropogenic GHG has continued to increase for the last 30 years; notably from 2000 to 2010, despite the growing number of mitigation policies. There is evidence in the continues increasing global warming in the last three decades successively at the Earth`s Surface, making it, the warmest three successive decades on the last 1400 years. (IPCC,2014)

The determination of radiative forcing allows to obtain the variation between the incoming solar radiation and the outgoing infrared radiation induced by the increased concentration of that gas. As a result, it is possible to analyse with this method the effect of the anthropogenic impacts and its connection to global warming. Their units are watts per square meter (W m^{2-}). A positive value of RF implies an increase of the superficial temperature and a negative value of RF indicates a reduction of the surface temperature. According to Figure 1, the total anthropogenic radiative value obtained in 2011 is 2.29 W m^{2-} and the emissions of carbon dioxide solely contributes 1.68. Therefore, carbon dioxide is considered the most relevant GHG so controlling its emissions and controlling the CO_2 stored in the atmosphere is crucial to mitigate the effects of global warming. A wide range of methods such as conservation and energy efficiency, renewable energy, nuclear energy, coal and gas substitution and carbon capture and storage must be established to adjust the increment of the demand of energy and mitigate the emissions of GHG. (IPCC, 2013)

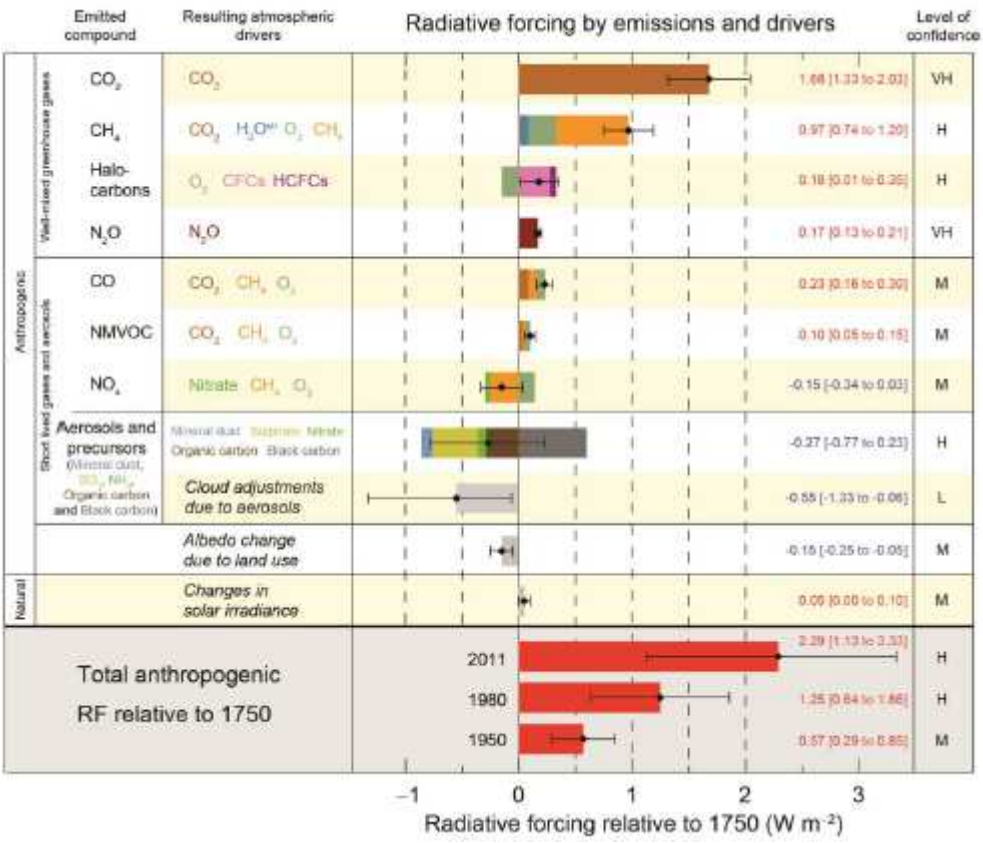

Figure 1. RF estimated over the period from 1750 until 2011, adding the uncertainties in whiskers shape. (IPCC, 2013).

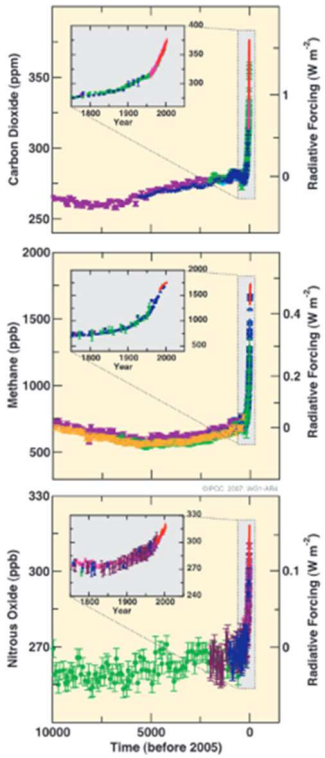

Figure 2. Atmospheric concentrations of carbon dioxide, methane and nitrous oxide during the last 10000 years. (IPCC, 2007)

1.1. Carbon Capture and Storage and its use to mitigate the CO_2 emissions.

Global emissions of CO_2 from fossil fuels have been increasing 2.7% annually over the last decade and are currently 60 % above the Kyoto Protocol. If no solutions and protocols are proposed to mitigate the GHG, the increasing growth rate will surely continue rising and the predicted temperature for 2100 will be between 3.7 and 4.8ºC. It has been estimated that to limit the increment of the temperature to 2ºC by 2050 at least a 50% of the carbon dioxide emissions should be reduced. (M. Cuéllar-Franca and Azapagic, 2015; IPCC, 2013)

Most of the models proposed by the Intergovernmental Panel on Climate Change's Fifth Assessment Report require carbon capture to stay within 2ºC of warming from pre-industrial days. If carbon capture isn't considered, emissions reduction costs would rise 138 percent. CCS is a worldwide used technology that controls the CO_2 emissions from fossil fuel-based power generation, which will experience continued growth especially in Asia (Global CCS institute, 2015). This technique consists of three steps: Capture, Transport and Storage. Carbon can be captured through three methods: Pre-combustion, Post-combustion and oxyfuel carbon capture. CCS can capture over 90% of the carbon dioxide emissions from powerplants and industrial facilities. Once it's captured it must be transported from its source to a storage point. Finally, carbon dioxide is injected into geological formations and kept stored underground.

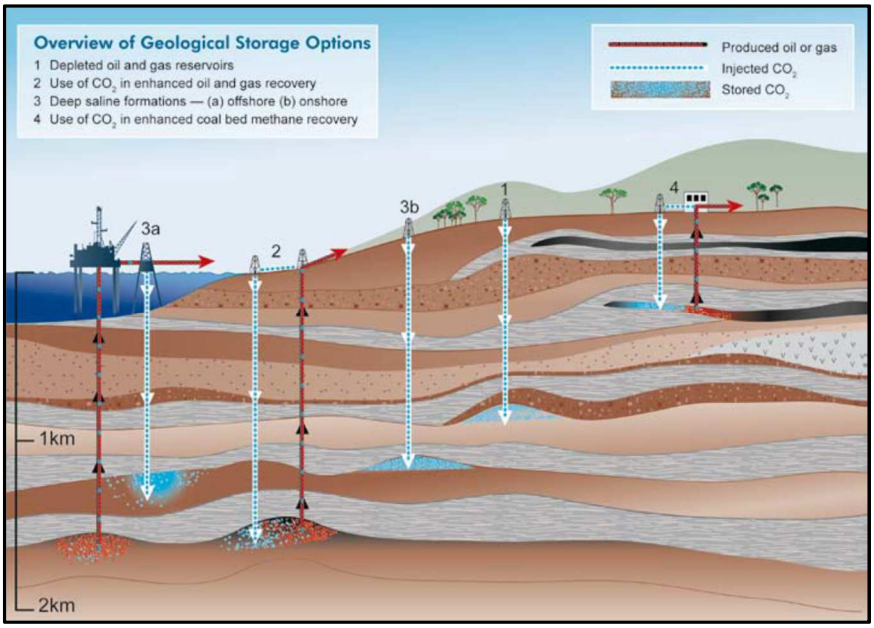

Figure 3. Carbon capture and storage process (IPCC,2005)

The International Energy Agency declares in the CCS technology roadmap in 2013 that it's necessary to support, encourage, prove and develop CCS technologies in the next seven years through seven steps in order to achieve the low-stabilization goals (IEA, 2013). These steps are:

- Introduce financial support mechanisms for demonstration and early deployment of CCS to drive private financing of projects.
- Implement policies that encourage storage exploration, characterisation and development for CCS projects.

- Develop national laws and regulations as well as provisions for multilateral finance that effectively require new-build, base-load, fossil-fuel power generation capacity to be CCS-ready.
- Prove capture systems at pilot scale in industrial applications where CO_2 capture has not yet been demonstrated.
- Significantly increase efforts to improve understanding among the public and stakeholders of CCS technology and the importance of its deployment.
- Reduce the cost of electricity from power plants equipped with capture through continued technology development and use of highest possible efficiency power generation cycles.
- Encourage efficient development of CO_2 transport infrastructure by anticipating locations of future demand centres and future volumes of CO_2.

Carbon capture can achieve 13 percent of the global greenhouse gas emissions reductions needed by 2050 and is viewed as the only practical way to achieve deep decarbonization in the industrial sector. However, if this technology fails in this usage for industrial sectors then this will be a large threat to the world's capacity to confront climate change. (IEA, 2015). Currently, at least 21 commercial-scale carbon capture projects are operating around the world with 22 more in development. Industries deploying large-scale carbon capture include coal gasification, ethanol production, fertilizer production, natural gas processing, refinery hydrogen production and, most recently, coal-fired power generation. (Center for climate and energy solutions(C2ES)

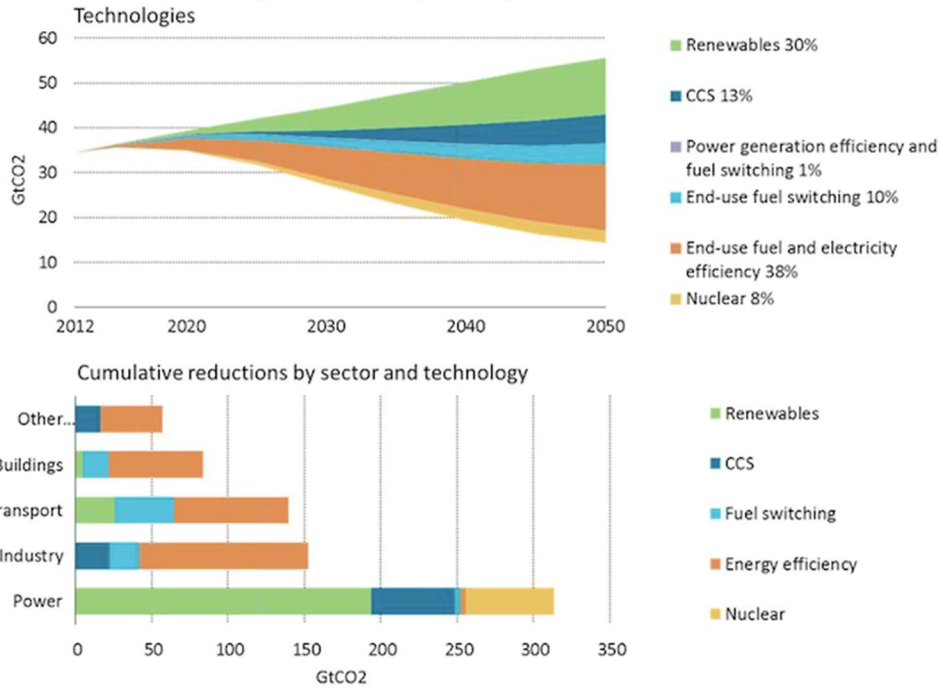

Figure 4. Contribution of sector and technology area to global cumulative CO_2 reductions between 6ºC scenario (6DS) and the 2ºC scenario (2DS).

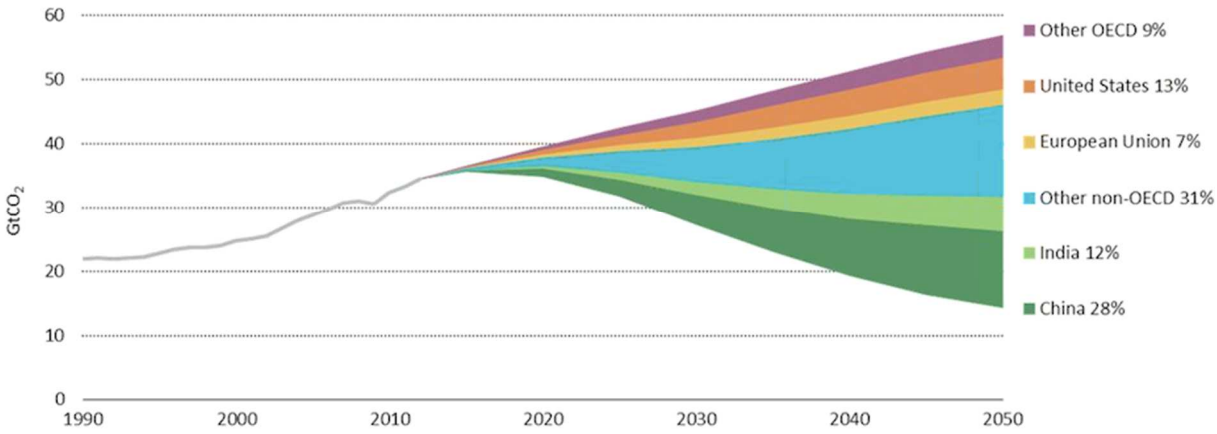

Figure 5. Contribution per regions to global cumulative CO_2 reductions between 6ºC scenario (6DS) and the 2ºC scenario (2DS).

1.2.Use of fly ashes for CO_2 sequestration

To avoid high CO_2 concentrations in the atmosphere, carbon dioxide can be separated from the fuel gas of industrial facilities, such as a power plant. Various technologies for carbon dioxide sequestration have been proposed, such as storage in empty gas fields, oceans and aquifers. An alternative sequestration route is the mineral CO_2 sequestration route in which CO_2 is chemically stored in solid carbonates by the carbonation of minerals. The alkaline industrial waste, such as fly ash can be considered a source of calcium and magnesium and therefore it can be used for the mineral sequestration of carbon dioxide (Jaschik et al. ,2016)

Fly ash along with bottom ash, boiler slag, fluidized-bed combustion ash is a Carbon Combustion Product (CCP). Fly ash corresponds to the 85% of the total ash produced during this process. The typical compositions of CCP are given in Table 3.

Table 3.Common range of elemental composition for Coal Combustion Products (CCP) from different coals, wt %. (Barnes, 2010; Heidrich et al., 2007).

Element	Bituminous	Sub-bituminous	Lignite
SiO_2	20-60	40-60	15-45
Al_2O_3	5-35	20-30	10-25
Fe_2O_3	10-40	4-10	4-15
CaO	1-12	5-30	15-40
MgO	0-5	1-6	3-10
SO_3	0-4	0-2	0-15
Na_2O	0-4	0-2	0-6
K_2O	0-3	0-4	0-4
LOI	0-15	0-3	0-5

Fly ash comprises the fine particles that rise along with the flue gases. Generally, it's not suitable for cementitious uses, however, the use of this material as a supplementary cementitious material has risen to 15 million tonnes in concrete in the USA (ACAA ,2006). Fly ash when used in conjunction with Portland cement contributes to the properties of the hardened concrete through hydraulic and pozzolanic activity. It's a finely divided amorphous alumino-silicate with varying amounts of calcium that when mixed with Portland cement and water produces calcium-silicates hydrates (C-S-H) and calcium-aluminate hydrates. The increment of the amount of the fly ash in concrete must be considered, as high-level fly ash cement may generate low early age strengths and delays in the rate of construction. The behaviour of fly ash in concrete is strongly influenced by its physical, mineralogical and chemical properties. The mineral and chemical composition depend on the composition of the coal. According to ASTM C618 Standard Specification for Coal fly ash and raw or calcined natural pozzolan use in concrete (AASHTO M295) there are two classes of fly ashes: ATSM class C and ATSM class F. (Portland Cement association, 2007)

The main difference between type F fly ashes and HCFA is the amount of calcium that it contains, as shown in Figure 6. Class F fly ashes commonly derive from bituminous and anthracite coals while HCFA derive from lignitic and sub-bituminous coals.

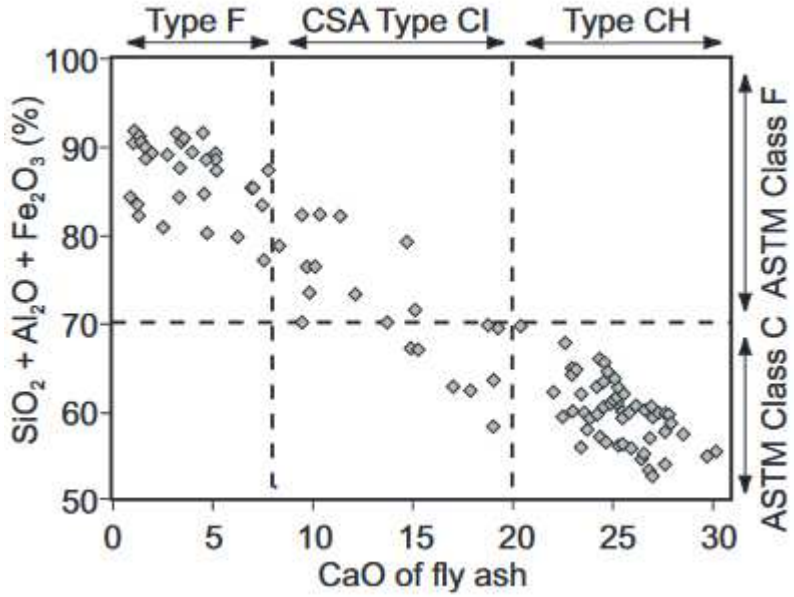

Figure 6. Correlation between the amount of CaO in fly ash and the sum of the oxides SiO_2 + Al_2O_3 and Fe_2O_3. (Thomas, 2007)

The calcium content of the fly ash indicates how it will behave in concrete. Class F fly ashes are generally composed of alumino-silicate glasses and crystalline phases that don't show any hydraulic behaviour. As a result, class F fly ashes only have pozzolanic properties. Moreover, these fly ashes require the presence of a cementing agent (alkali or lime), such as calcium hydroxide, to react and form cementitious hydrates. HCFA have a higher quantity of calcium and these are composed of calcium-alumino-silicate glass and a wider range of crystalline phases than class F fly ashes. Some of these crystalline phases react rapidly with water and harden during the process. HCFA doesn't require an agent to react and form cementitious hydrates and therefore this fly ash has pozzolanic and hydraulic properties. (Thomas, 2007)

The use of fly ashes as a filler in concrete reduces the water demand, due to the reduction of the permeability and as a result it enhances the durability of the concrete. However, these benefits highly depend on the content of carbon and its fineness. A coarser fly ash with a high content of carbon must be considered before using it as a replacement of structural concrete, especially at elevated levels. (Thomas, 2007)

Class F fly ashes have generally been used to mitigate the deleterious expansion of the alkali-silica reaction (ASR) and are usually proved to be effective when used in sufficient doses. In contrast, High Calcium Fly Ashes or Class C fly ashes tend to be less effective and require higher dosages if they can be used at all. (Rachel Detwiler, 1997)

The total current fly ashes production has gradually increased since 2002 from 500 million tonnes to values amongst 600 and 650 million tonnes. However, not all of fly ashes produced worldwide are utilized. Only an 80% of class F fly ashes are used and minor amounts of HCFA, approximately 20%, are used. (Uliasz-Bocheńczyk et al., 2015). Despite the lower use of HCFA, this fly ash can be economically useful to reduce CO_2 emissions from the professional power industry via mineral carbonation. (Uliasz-Bocheńczyk et al., 2009)

Table 4.Chemical composition of the coal fly ash dependent of the region. (Blissett & Rowson,2012)

Component	Range (mass%)				
	Europe[a]	US[b]	China[c]	India[d]	Australia[e]
SiO_2	28.5–59.7	37.8–58.5	35.6–57.2	50.2–59.7	48.8–66.0
Al_2O_3	12.5–35.6	19.1–28.6	18.8–55.0	14.0–32.4	17.0–27.8
Fe_2O_3	2.6–21.2	6.8–25.5	2.3–19.3	2.7–14.4	1.1–13.9
CaO	0.5–28.9	1.4–22.4	1.1–7.0	0.6–2.6	2.9–5.3
MgO	0.6–3.8	0.7–4.8	0.7–4.8	0.1–2.1	0.3–2.0
Na_2O	0.1–1.9	0.3–1.8	0.6–1.3	0.5–1.2	0.2–1.3
K_2O	0.4–4	0.9–2.6	0.8–0.9	0.8–4.7	1.1–2.9
P_2O_5	0.1–1.7	0.1–0.3	1.1–1.5	0.1–0.6	0.2–3.9
TiO_2	0.5–2.6	1.1–1.6	0.2–0.7	1.0–2.7	1.3–3.7
MnO	0.03–0.2	nd	nd	0.5–1.4	nd
SO_3	0.1–12.7	0.1–2.1	1.0–2.9	nd	0.1–0.6
LOI	0.8–32.8	0.2–11.0	nd	0.5–5.0	nd

Table 5. Major elements and trace elements in fly ash according to various authors. (Shaheen et al.,2012)

Element	Coal fly ash						
	Page et al. (1979)	Adriano et al. (1980)	Jala and Goyal (2006)	Tripathi et al. (2009)	Pandey et al. (2009)	Riehl et al. (2010)	Lopareva-Pohu et al. (2011)
Major elements, g kg^{-1}							
Al	1–17.3	–[a]	312	–	4.8	108.5	0.47
Ca	1.1–222	5.4	34	0.029	–	86.4	1.84
Fe	10–290	16	68	0.0032	4	36.6	0.31
K	1.5–35	1.8	10.8	0.072	–	24.5	0.0021
Mg	0.4–76	1.2	1.4	0.017	–	11.5	0.019
P	0.4–8	0.5	10.8	0.0027	1.1	2.1	0.0024
S	1–15	20	0.02	0.058	–	2	0.013
Trace elements, mg kg^{-1}							
As	2.3–6300	–	6.2	BLD[b]	–	–	20.4
B	10–618	50	–	–	28.9	–	0.40
Cd	0.7–130	1.3	1.9	13.4	42.5	0.03	–
Co	7–520	7	58	21.1	–	26	17
Cr	10–1000	15	330	38.2	40.3	148	46
Cu	14–2800	19	0.002	65.8	58.4	57	38
Hg	0.02–1.0	0.18	–	BLD	–		0.40
Mn	58–3000	100	739	0.006	69.3	679	418
Mo	7–160	3.0	4.0	–	33.3	4.2	–
Ni	6.3–4300	15	13	44.2	204.8	88	48
Pb	3.1–5000	16	35	20.0	40.2	97	39
V	–	20	–	–	–	182	–
Se	0.2–134	3	3.6	–	–	–	–
Zn	10–3500	39	79	57.7	82.3	167	85

[a] Not measured.
[b] BLD – below the limit of detection.

Fly ashes can capture the emissions of CO_2 through absorption and carbonation. (Gray et al., 2004; Mercedes Maroto-Valer et al., 2008).

The capture through absorption occurs with the reaction between carbon dioxide and the surface of the fly ash. As a result, the high superficial area of the fly ash can provide the required site for CO_2 absorption. (Ahmaruzzaman, 2010). However, when the temperature is 120ºC or above the reaction is reversed as carbon dioxide is released back to the atmosphere when the surface of fly ash is activated by heating. (Siriruang ,2016)

The capture through carbonation occurs when the free oxide compounds react with carbon dioxide and form carbonates (Chowdhury et al., 2013). The carbonation reaction of calcium oxide is the main reaction for fly ashes. This reaction is shown in equation 1. There are other oxide compounds on the fly ash which can also carbonate, such as magnesium oxide, but in minor cases as these compounds aren't as reactive as calcium oxide. Class F fly ashes tend to not carbonate as much as HCFA due to the lower content of calcium oxide. The carbonation reaction is exothermic, and it occurs spontaneously in nature. The reaction is reversible at the temperature of 750-950ºC due to the decomposition of $CaCO_3$. (Siriruang ,2016)

$$CaO + CO_2 \rightarrow CaCO_3 \qquad \textbf{(1)}$$

The free CaO contained in fly ash can be transformed into $Ca(OH)_2$ in the presence of moisture content in the atmosphere (Dubina et al., 2013). This process is known as hydration and it can occur under atmospheric pressure and room temperature conditions. This reaction is shown in equation 2.

$$CaO + H_2O \rightarrow Ca(OH)_2 \quad \textbf{(2)}$$

Calcium hydroxide can further react with CO_2 to form $CaCO_3$.This reaction is the same process shown in equation 1, since it generates calcium carbonate. However, in this case it binds CO_2 with calcium hydroxide, due to the hydration process mentioned above, in equation 2. The reaction is shown in equation 3. (Siriruang ,2016)

$$Ca(OH)_2 + CO_2 \rightarrow CaCO_3 + H_2O \quad \textbf{(3)}$$

The use of carbon dioxide via carbonation can help to reduce the free CaO content in fly ash. Therefore, carbon dioxide can benefit the use of fly ash as a mineral admixture in concrete. (Siriruang ,2016)

The amount of free CaO which reacted with CO_2 in the capture process by carbonation can be determined through the comparison of Ca^{+2} ions in aqueous solution of fresh fly ash and that of the fly ash after the CO_2 capture. (Siriruang ,2016)

Free Ca^{+2} consumption by the carbonate reaction is shown in equation 4. The amount of free calcium of the sample is important during an experiment as it allows to know which pressure and temperature you must introduce into the system in order to leap calcium oxide from the fly ash. If the amount of the free calcium is low, then it requires a higher pressure and temperature to produce carbonation.

$$\text{Free } Ca^{2+} \text{ consumption } (\%) = \frac{Free\ Ca^{2+}_{initial} - Free\ Ca^{2+}_{left}}{Free\ Ca^{2+}_{initial}} \quad \textbf{(4)}$$

2 Objectives

The impact generated by global warming is increasing due to the anthropogenic emissions of GHG, mainly of carbon dioxide. Protocols and solutions are required to mitigate the GHG. During the Paris summit 2015 it was established that to control and limit the global warming to the 2ºC scenario, a wide range of low-carbon technologies was required. Low-carbon technologies involve the use of renewable energies, nuclear energy and carbon capture and storage (CCS). CCS is considered essential to minimize the CO_2 emissions from industrial sectors as it traps this gas permanently into stable carbonate minerals.

The aim of this thesis is the feasibility study of the carbonation reaction of high calcium fly ashes. These residues are formed during the combustion of coal and have been proven to be useful for the carbon dioxide sequestration. This is due to the presence of calcium oxide and magnesium oxide which can react with carbon dioxide to form calcium and magnesium carbonate. However, this reaction tends to be linked more with the amount of calcium oxide as it's more reactive than magnesium oxide. This study will be focussed on the analysis of two different fly ashes with a distinctive content of calcium. These samples will be exposed to 1bar CO_2 and will be analysed modifying two parameters, temperature and the moisture content, that can influence the carbonation process.

The rate of carbonation and the kinetics of these reactions are estimated qualitatively by the main characteristic peaks of the X-ray powder diffraction (XRD) spectrum given before and after carbonation. The high resolutions images provided by the Scanning electron microscopy (SEM) are used to identify the variations in the chemical composition of the fly ash before and after carbonation.

3 Experimental procedure

3.1 Instrumentation setup

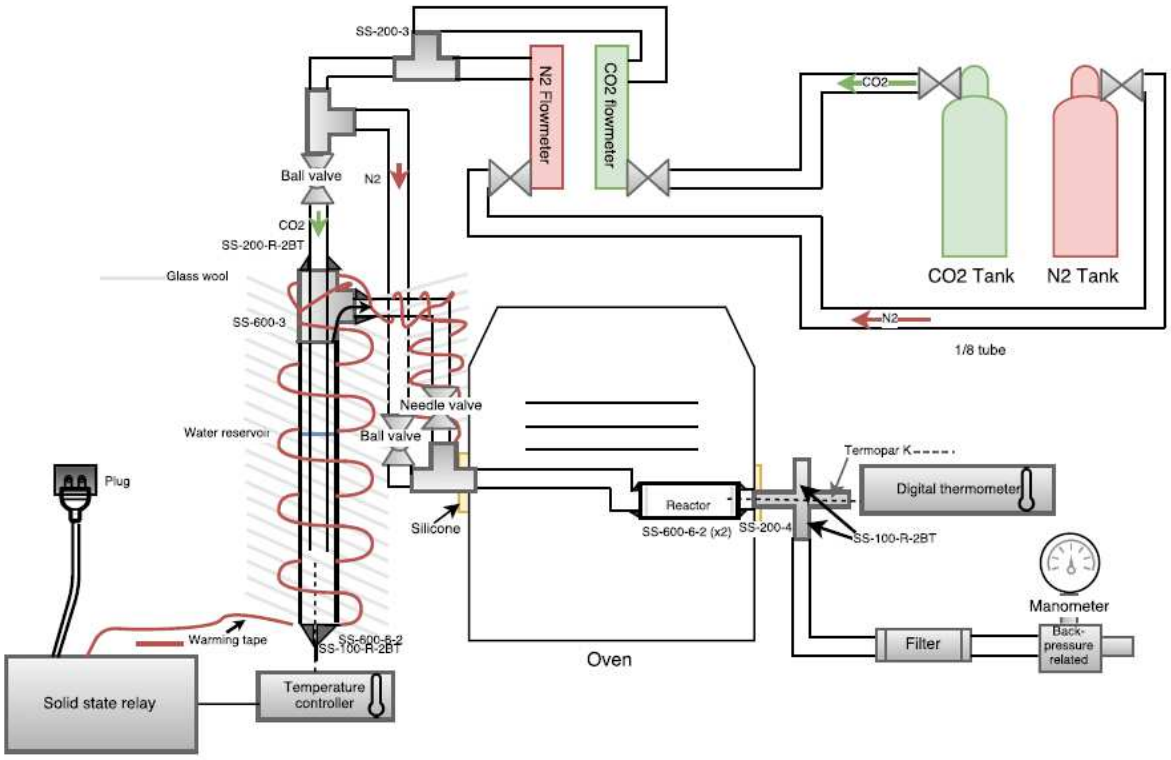

Figure 7. Schematic of the reactor, where the carbonation experiment took place.

The sample is placed inside in a 3/8-inch tubular reactor located inside an oven and both ends are blocked with glass wool to keep the sample thermically insulated but allowing the gas to flux inside it, as shown in Figure 7. The flow of this gas is introduced into the system and it's regulated with the flowmeter. Nitrogen is used as a carrier gas and it allows you to reach the needed conditions for the experiment. On the other hand, Carbon Dioxide is used during the experiment to generate the carbonation process inside the reactor. For the conditions of this thesis, dry and wet conditions are used in order to analyse how the presence of water affects the carbonation process. For wet-conditions experiments, water vapour is produced inside the water reservoir, due to the modification of the temperature inside the bubbler via temperature controller.

The ball valve and the needle valve located on the left side of the oven are used to control the gas flux introduced inside the oven. To ensure there is no gas leakages PTFE tape is used on the ball valves.

The gas that exits the reactor is connected to a digital thermometer and a manometer which are used to determine the temperature and the pressure inside the reactor. For the conditions of this thesis, the temperature inside the reactor is modified in order to analyse the effects it has on the carbonation of fly ashes. The pressure inside the reactor shall

remain constant (1 bar). On the right side of the oven there is a back-pressure which is used to regulate the pressure once the experiment has ended. This device can only sustain a maximum pressure of 6.8 bars, so controlling the pressure of the system is necessary to avoid any further damage. Throughout the experiment, the implementation of fittings and ferrules has been required. The ferrules used for our system are mainly made of stainless steel except for the capillary ferrules used to connect the thermocouple K to the system which are made of graphite. Graphite ferrules are more soft and malleable and can extrude into shape to fill minor imperfections. The fittings used are made of stainless steel. Other material that have been used for the experiment are Glass wool and Silicone which are mainly used as thermal insulators.

3.2 Information of the samples used for the experiment

The samples used for this experiment come from a thermoelectric powerplant located in Andorra, located in the east of Spain in Teruel (Aragon) and from Ptolemais power plant, which is in Kozani, Greece.

Andorra coal-fired powerplant produces annually over 1,000.000 tons of coal ash (15% bottom ash-85% fly ash) that are stored in the Valdeserrana dam. The chemical composition of these fly ashes indicates a low calcium content (below 10%), as shown in Table 6, and therefore Andorra fly ashes are classified as a class F fly ash. (Goumans et al.,1994; Goumans et al.,1997)

Ptolemais power plant produces most of the total annual fly ash in Greece (about $7.6x10^6$ tons out of, the total produced in Greece over the last two years, $10x10^6$). Ptolemais is rich in calcium compounds for that reason it's considered a fly ash type C (approximately 30%). (Skodras et al.,2005). According to the European Normative, Greece along with Spain and Poland is one of the main producers of high calcium fly ash. This is the main motive why we decided to analyse fly ashes from the Ptolemais Powerplant. Spanish fly ash was analysed in order to compare and distinguish the difference between the two types of fly ashes.

Table 6. Chemical composition of the fly ashes from Andorra.

Oxides	Chemical composition fly ashes Andorra (%)	Chemical composition fly ashes Ptolemais (%)
MgO	1.50	-
Al_2O_3	24.70	-
SiO_2	40.60	21.40
P_2O_5	0.40	-
SO_3	0.60	4.20
K_2O+Na_2O	1.50	1.20
CaO	8.30	22.00
Fe_2O_3	20.00	-
TiO_2	0.80	-
SrO	0.10	-
LOI (Loss on ignition)	1.70	-

3.3 Scanning Electron Microscopy (SEM) and Energy Dispersive X-ray (EDX) spectroscopy

Scanning electron Microscopy (SEM) is a type of electron microscope that uses a focused beam of high-energy electrons and it's used to scan across the surface of solid specimens. The signals that are produced from electron-sample interactions reveal information about the crystalline structure, chemical composition and external morphology. By scanning simultaneously in two perpendicular directions, a square or rectangular area of specimen (known as a raster) can be covered and an image of this area can be formed by collecting secondary electrons from each point on the specimen.
SEM is mainly used to generate high-resolution images of objects and to show spatial variations in chemical compositions. It can also identify precisely phases based on chemical analysis or chemical structures with sizes down to 50 nanometers (nm).

Modern SEM provides an image resolution typically between 1 and 10 nm and a relatively large depth of focus: specimen features that are displaced from the plane of focus appear almost sharply in focus.

An Energy Dispersive X-ray (EDX) analyser is used to identify the elemental composition of these particles and provide a quantitative compositional information.

3.4 Preparation and conditions for our experiment

For our experiments we used the instrument EMITECH K950X and Phenom XL equipped with a chamber that allows analysis of large samples up to 100mm x 100mm at the Barcelona Research Center in Multiscale Science and Engineering, BRCMSE (multiscale.upc.edu).

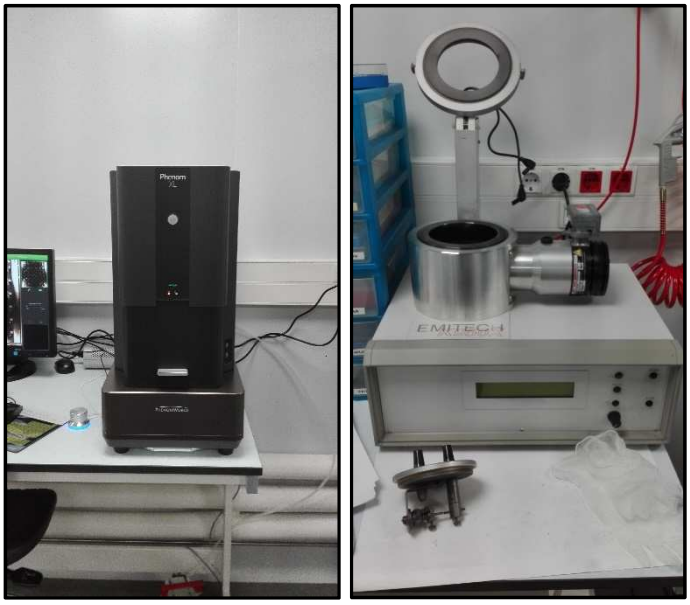

Figure 8. On the left, Phenom XL and on the right EMITECH K950X at the BRCMSE.

The powder material was located on top of the stub after placing the carbon tap. The EMITECH K950X was programmed alternating the evaporation parameter mode by using

the value multi-pulse. The evaporator time used for the experiment was 950 milliseconds and the vacuum used is $3x10^{-3}$ bars. The carbon gun works with two carbon rods. One of them must be placed flat into the carbon gun and must be fitted and fixed with the screw and the other terminal must be sharpened for one centimetre till its diameter is approximately 1mm.This terminal allows the movement of the rod. This process is necessary to obtain the correct evaporation parameters. (Quorum technologies,2008)

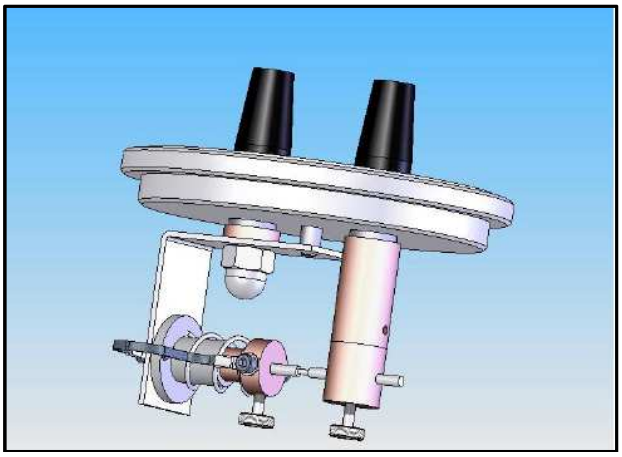

Figure 9. Carbon gun assembly. (Quorum technologies,2008)

The samples were then adjusted in a sample holder and the height was regulated to 2 mm as it was the necessary base distance required for a SEM analysis. For SEM imaging, we changed the mode from normal to SEM generating more vacuum in the process. This equipment has three detectors, Back Scattering Detector (BSD), Energy Dispersive Spectroscopy (EDS) system and Secondary Electron Detector (SED). It is also possible to control other parameters such as the intensity of the beam, the image resolution and the magnification used.

3.5 X-ray diffraction technique(XRD)

X-ray diffraction is a rapid analytical technique used for phase identification of a crystalline material. The regular distribution between the atomic spacing of the mineral conforms a crystal structure defined by the repetition of the unit cell in the form of a paralleliped. It contains all the information of the unit cell dimensions.

The crystal structure is represented by reticular planes uniformly spaced in different orientations represented by the Miller Indices (h, k, l). The distance between the planes is expressed as $d_{hkl.}$ The distance determines the position of the diffractions peaks using the Bragg Law which calculates the angle where constructive interference x-rays scattered by parallel planes of atoms, as follows:

$$\lambda = 2d_{hkl} \cdot \sin\theta \qquad \textbf{(5)}$$

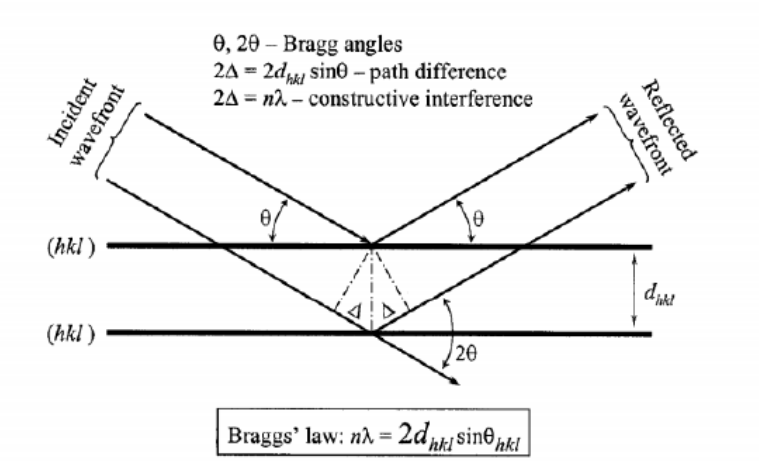

3.6 Preparation and conditions for our experiment

For our experiments we used the instrument Buker D8 Advanced, equipped with a theta-theta goniometer with a rotating sample holder, at UPC's Barcelona Research Center in Multiscale Science and Engineering (BRCMSE).

Figure 10. Buker d8 Advanced used for XRD at the BRCMSE

The powder material was pressed manually by means of a glass plate to get a flat surface in a cylindrical sample holder. The range of analysed angles goes from 10º to 80º using a step-size of 0.02º and measuring time of 1 seconds per step.

3.7 Carbonation procedure

Each sample is exposed to 1 bar of CO_2 and atmospheric pressure. The sample is introduced inside the reactor in where both extremes are blocked with glass wool in order to keep the sample thermically insulated. The temperature and moisture content will be modified as shown in Table 7. To achieve the ideal conditions for the experiment, the temperature is raised at a constant rate of 5 degrees per minute, injecting nitrogen with a flux of 55 ml/min, until achieving the required temperature for the experiment. If the experiments are done under wet conditions, the temperature controller is first raised to 60ºC and once the water is introduced inside the bubbler the temperature controller is programmed to 88ºC. This temperature allows to achieve the same quantity of water

vapour and carbon dioxide inside the reactor. Once it reaches the desired temperature inside the reactor, the nitrogen injection is cut off and CO_2 is injected into the system with a flux of 55 ml/min. The time for each carbonation experiment is 2 hours and once it's over, carbon dioxide is cut off and nitrogen is introduced into the system.

Table 7.Sample and water reservoir properties for each experiment." And" stands for Andorra and "PT" for Ptolemais.

	Sample properties				**Bubbler (Water reservoir)**		Carrier gas
Sample Name	Temperature (ºC)	Pressure (bars)	Flux (ml/min)	Time (h)	Water quantity (ml)	Temperature of water (ºC)	N_2 (bars)
And-1	160	1	55	2	-	-	1
And-2	220	1	55	2	-	-	1
And-3	160	1	55	2	20	88	1
PT-1	160	1	55	2	-	-	1
PT-2	220	1	55	2	-	-	1
PT-3	160	1	55	2	20	88	1

Table 8. Mass of the sample in grams before and after carbonation.

	Before Carbonation	**After Carbonation**
Sample Name	Mass of the sample (g)	Mass of the sample (g)
And-1	1.9903	1.6700
And-2	1.9070	1.6900
And-3	2.1410	1.9100
PT-1	1.6952	1.1260
PT-2	1.8440	1.7790
PT-3/2	1.8240	1.4170

The mass losses can be attributed to human factor and the sample got stuck on the glass wool.

4 Results

All the samples are analysed before and after carbonation with X-Ray Diffraction (XRD) and Scanning electron microscopy (SEM), to understand the carbonation reaction that has taken place on the reactor.

4.1 Scanning Electron Microscopy (SEM) and Electron Dispersive X-ray (EDX) spectroscopy

The morphology of the un-carbonated Coal Fly Ash (CFA) particles studied using SEM is shown in Figure 11. The CFA particles shown are cenospheres, which are generally present in fly ash, and vesicular particles which are formed due to the presence of gases and vapours. From these results we can observe a fluctuation of the size and shape of the cenospheres. The size of these particles varies from very large particles to smaller ones. The shape of the cenospheres tends to be spherical though some angular particles can also be observed. Cenospheres are mainly composed of aluminosilicate though it is possible to find iron-rich spheres too.

Table 9-18 give information about the chemical composition of samples PT/1, PT/2 and And/3. Generally, most of the particles analysed by EDX gave us the same elements but in different contents. Figure 12-14 and 32-34 correspond to Andorra fly ash. The main elements detected are: Oxygen, Calcium, Carbon, Silicon and Aluminium. Figure 15-17 and 21-31 correspond to high calcium fly ash. The main elements detected are: Iron, Oxygen, Calcium, Carbon and Silicon.

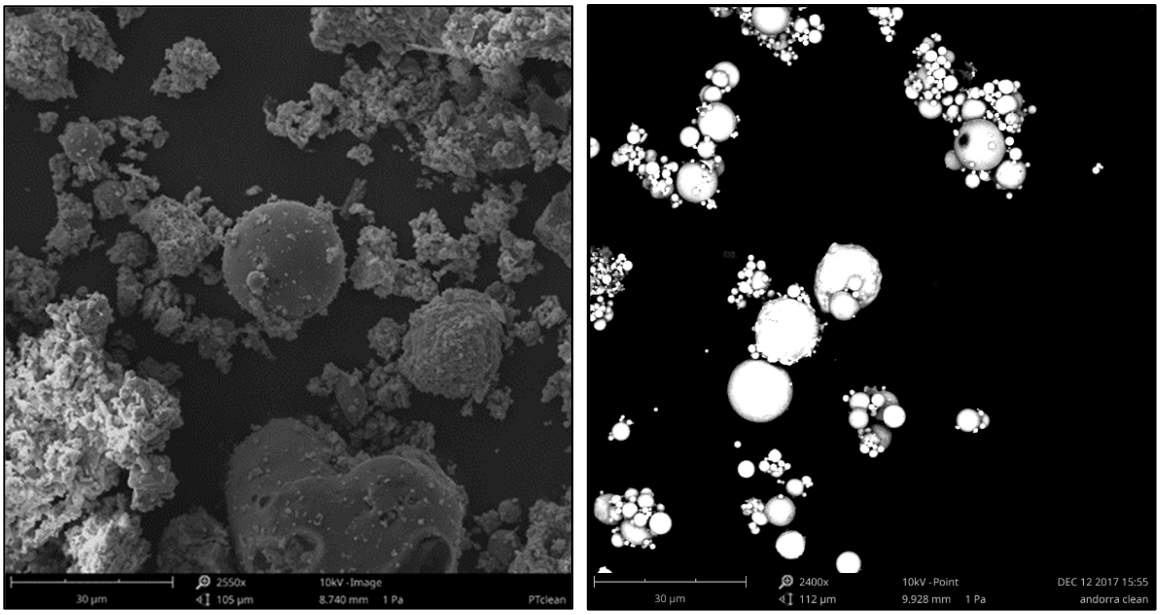

Figure 11.SEM image of the uncarbonated Ptolemais and Andorra Fly ash

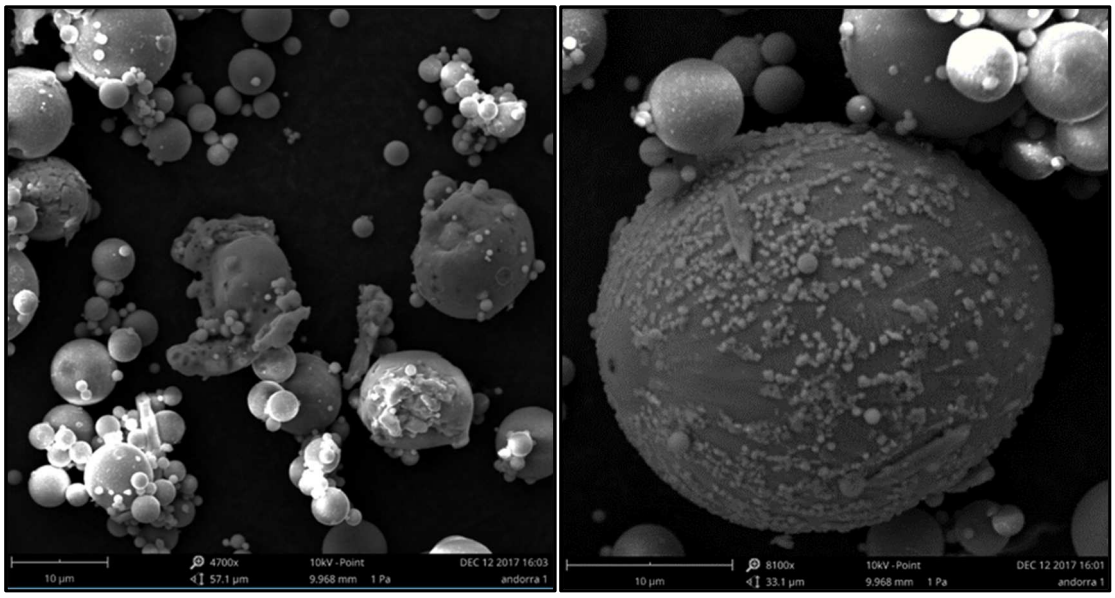

Figure 12.SEM image of the cenospheres of the Andorra fly ashes after carbonation under dry conditions and a temperature of 160º C.

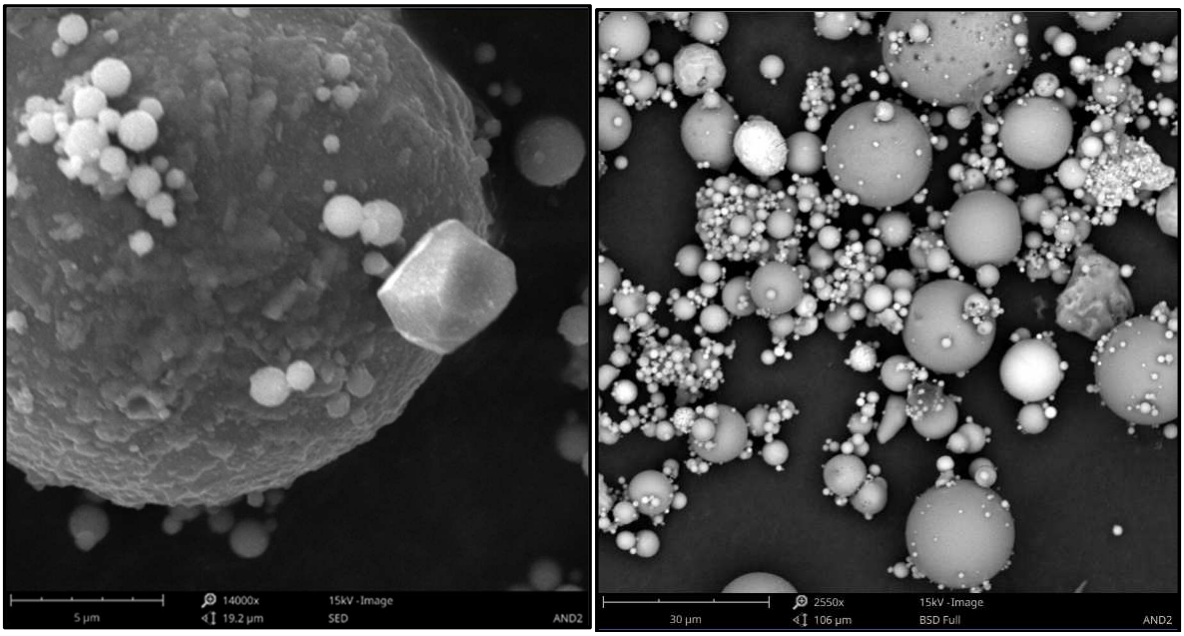

Figure 13.SEM image of the cenospheres of the Andorra fly ashes after carbonation under dry conditions and a temperature of 220º C.

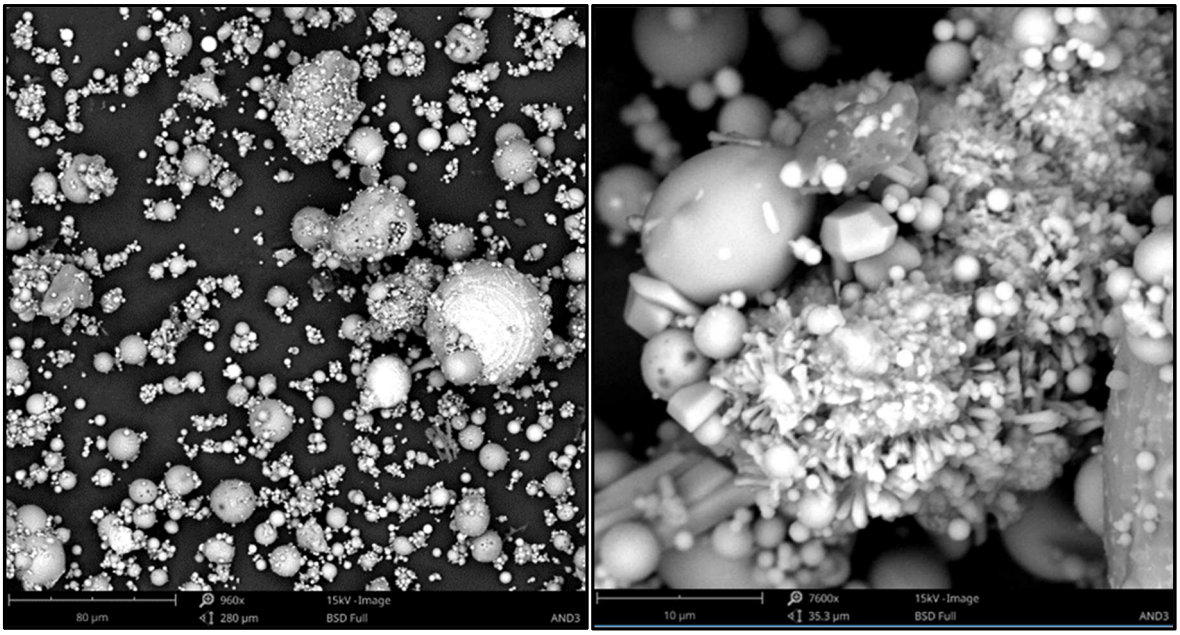

Figure 14.SEM image of the cenospheres of the Andorra fly ashes after carbonation under wet conditions and a temperature of 160ºC.

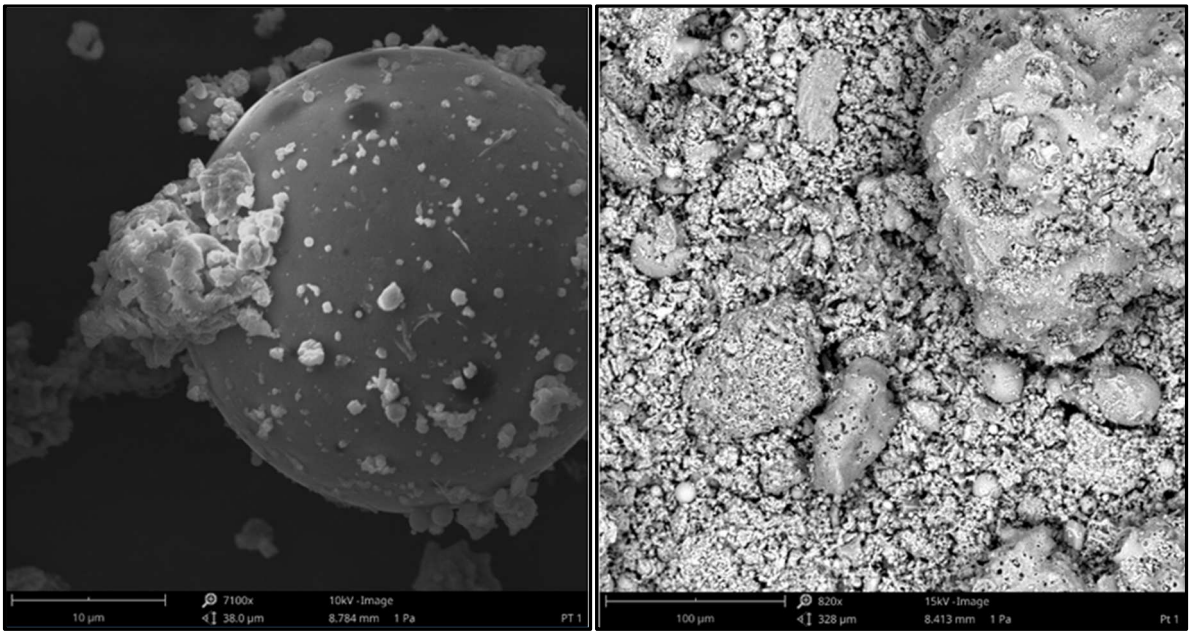

Figure 15. SEM image of the cenospheres of the Ptolemais fly ashes after carbonation under dry conditions and a temperature of 160º C.

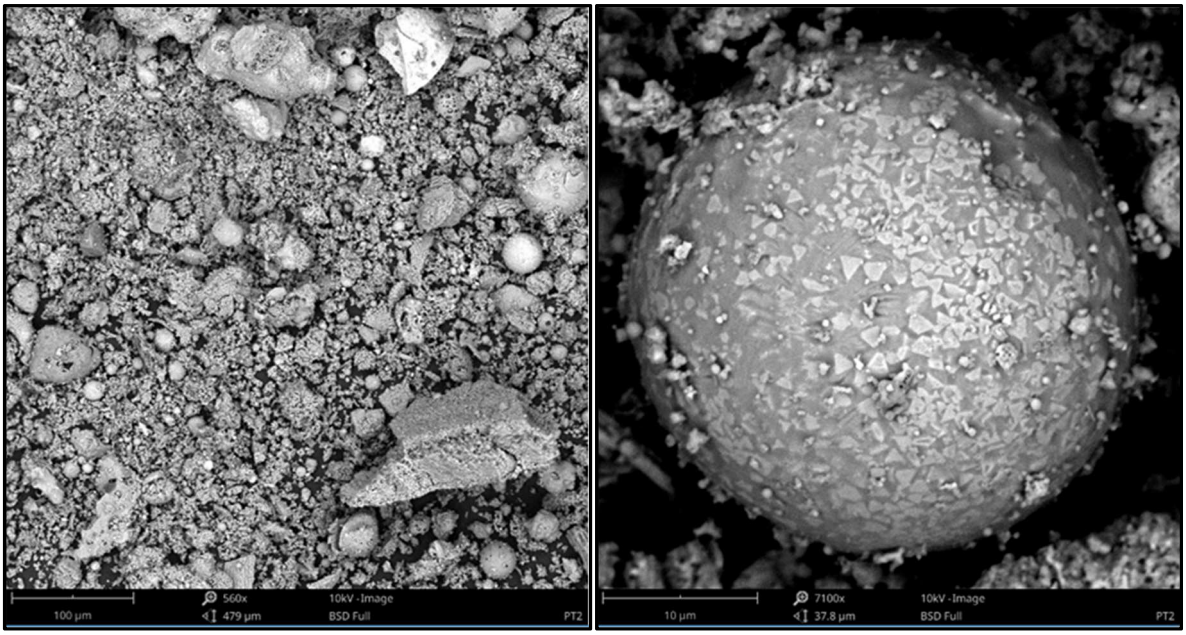

Figure 16.SEM image of the cenospheres of the Ptolemais fly ashes after carbonation under dry conditions and a temperature of 220º C.

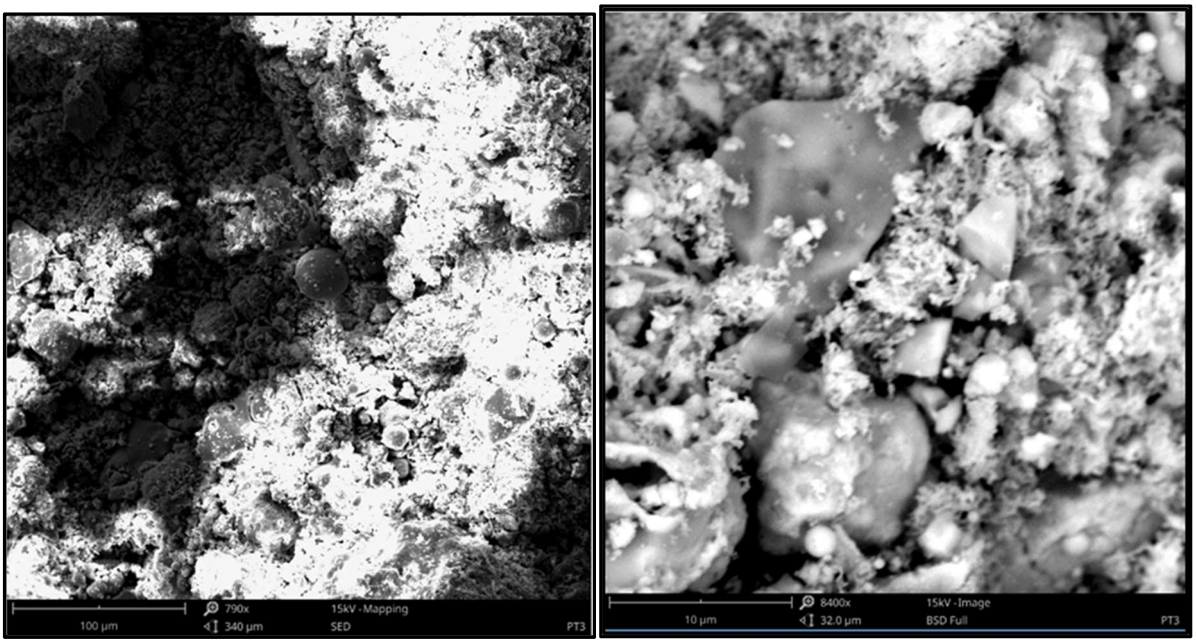

Figure 17.SEM image of the cenospheres of the Ptolemais fly ashes after carbonation under wet conditions and a temperature of 160º C.

4.2 X-ray diffraction

The XRD pattern of the fly ashes before and after carbonation (dry and wet) is shown in Figure 18 and Figure 19. By defining peak areas and/or intensities (counts), it is possible to compare the difference between the spectrums before and after carbonation. The range of analysed angles goes from 10º to 75º.

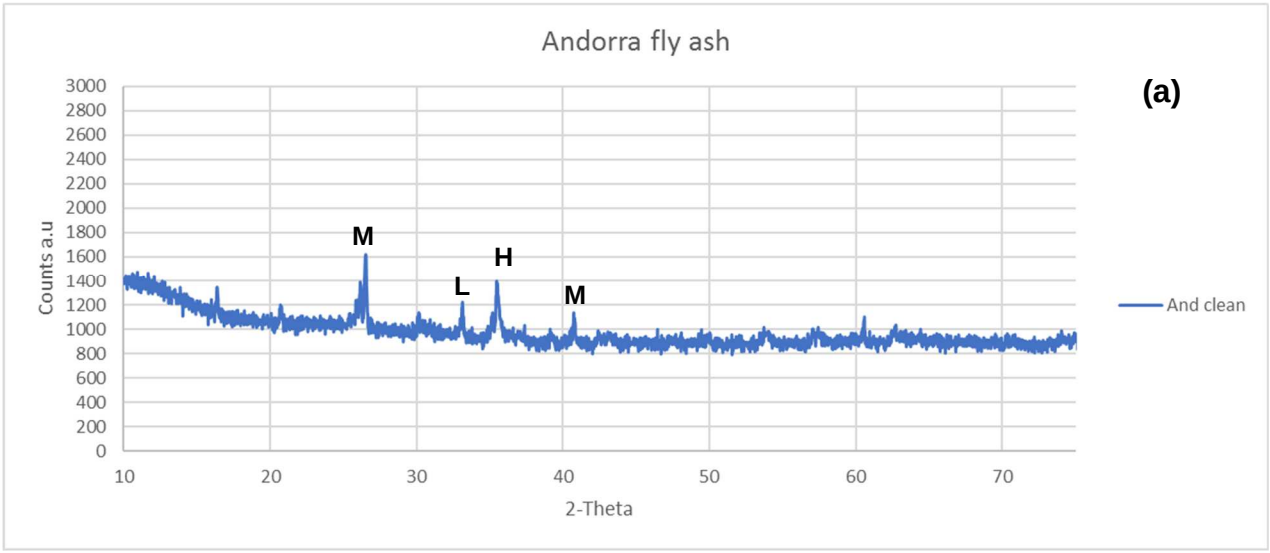

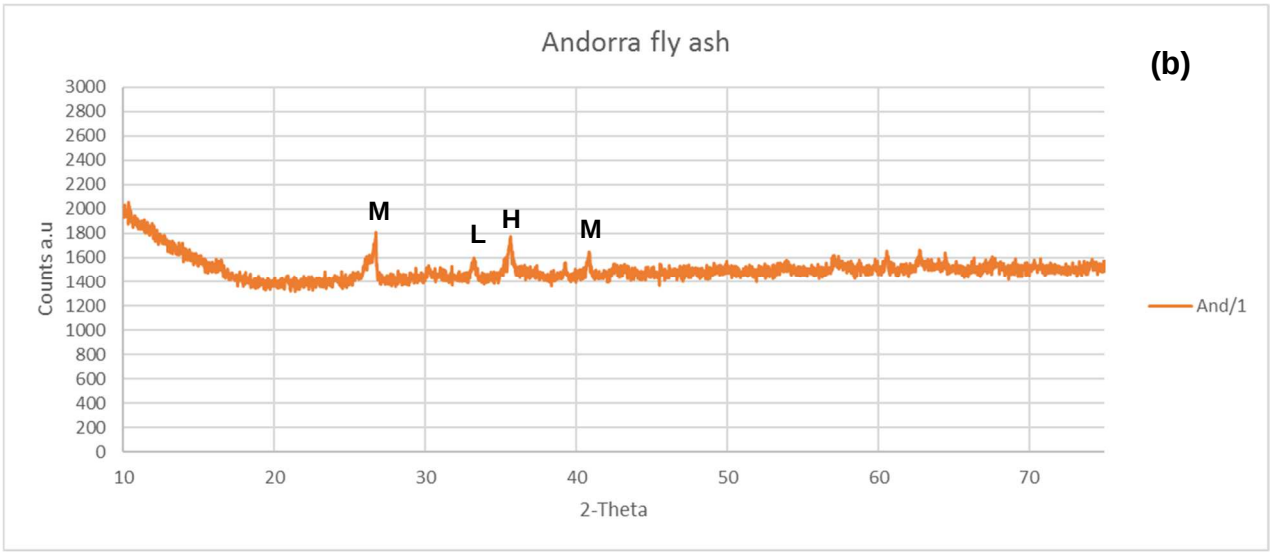

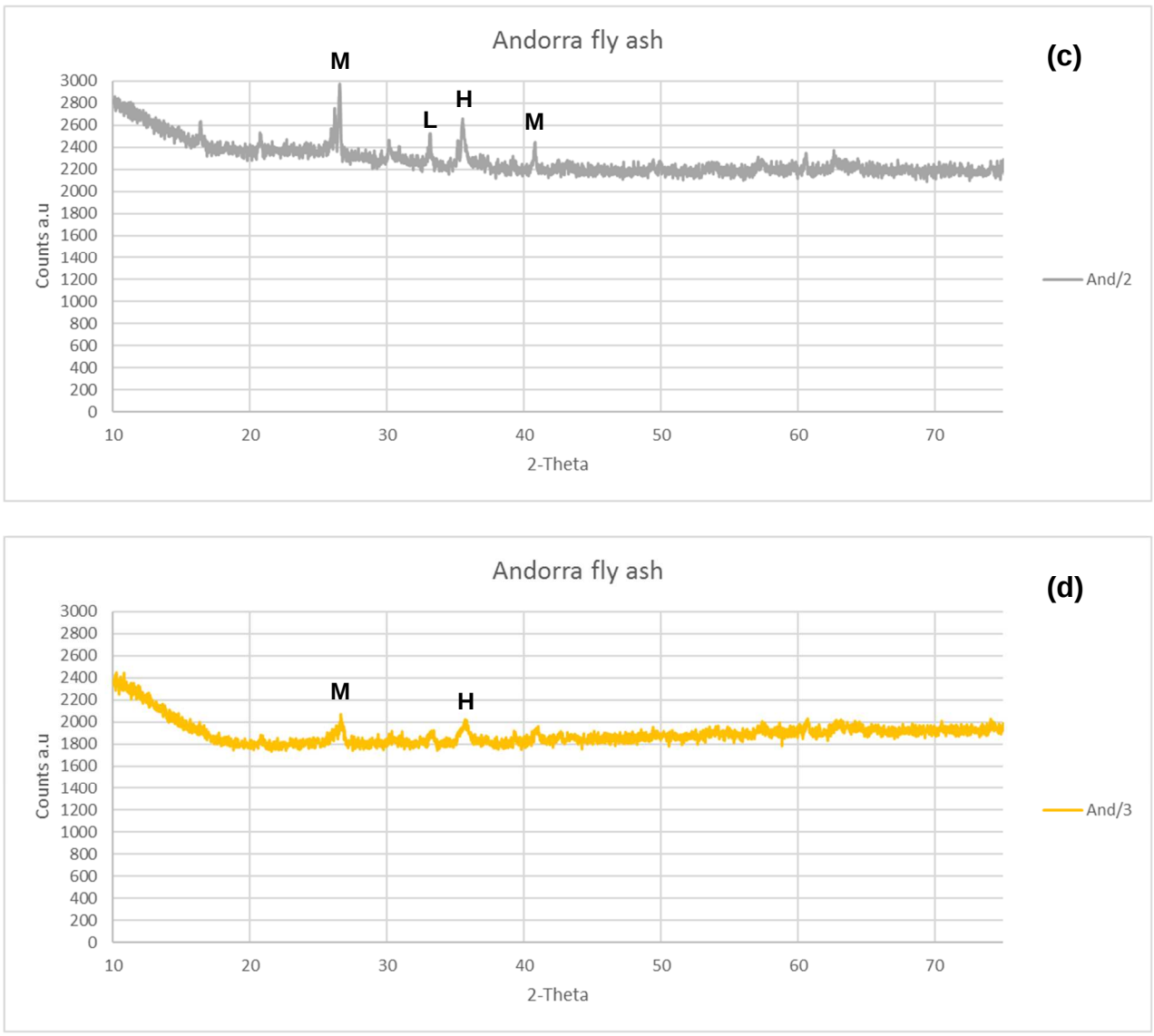

Figure 18.XRD pattern of the Andorra fly ashes after and before carbonation. (a) Before carbonation (b)After carbonation. Dry conditions.160ºC (c)After carbonation. Dry conditions. 220ºC (d) After carbonation. Wet conditions. 160ºC. M=Mullite (Al_2SiO_3) H=Hematite (Fe_2O_3) L=Lime (CaO)

From the XRD peaks of the Andorra fly ashes, the mineral phases identified are mullite, lime and hematite. The peak of lime is completely absent in the wet carbonated sample, as shown in Figure 18(d).

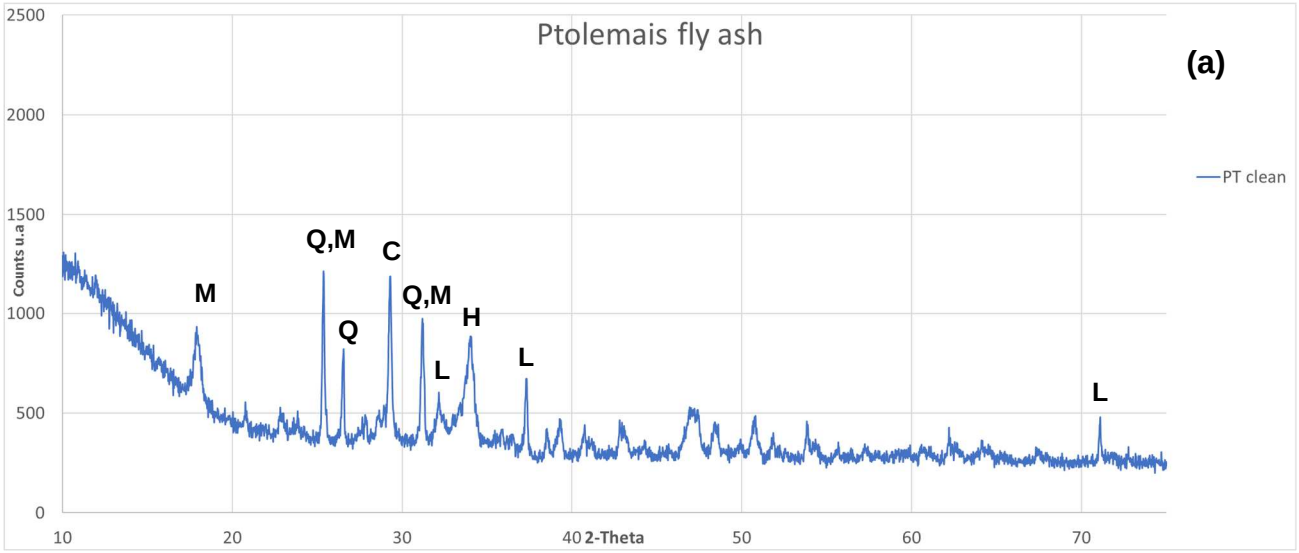
Ptolemais fly ash
(a)
PT clean
Counts u.a
2-Theta
M
Q,M
Q
C
Q,M
H
L
L
L

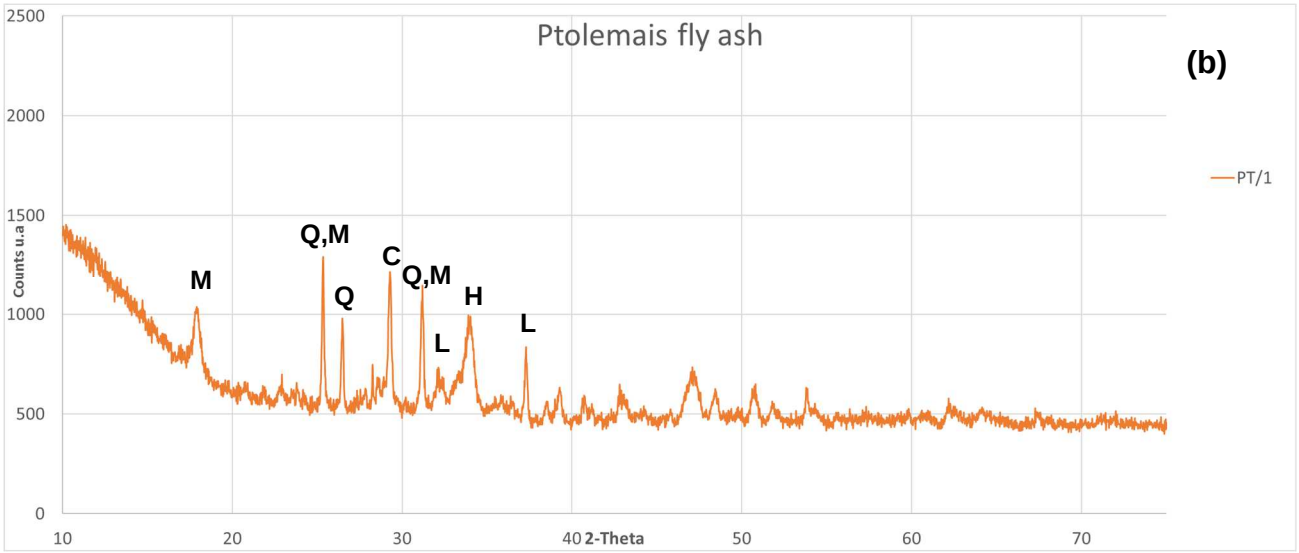
Ptolemais fly ash
(b)
PT/1
Counts u.a
2-Theta
M
Q,M
Q
C
Q,M
H
L
L

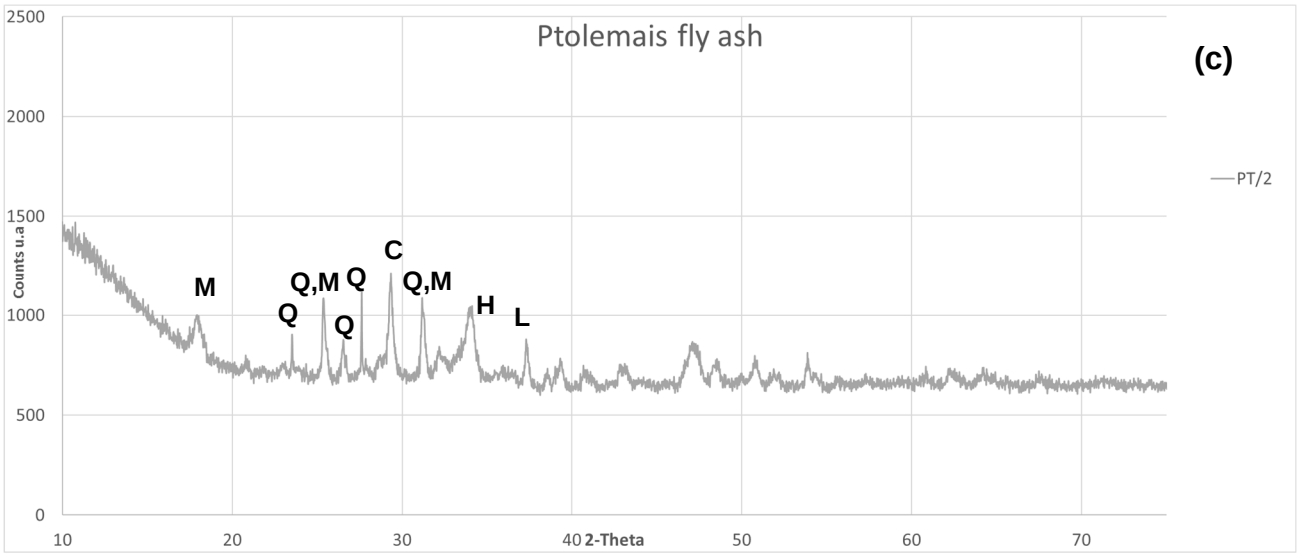
Ptolemais fly ash
(c)
PT/2
Counts u.a
2-Theta
M
Q
Q,M
Q
Q
C
Q,M
H
L

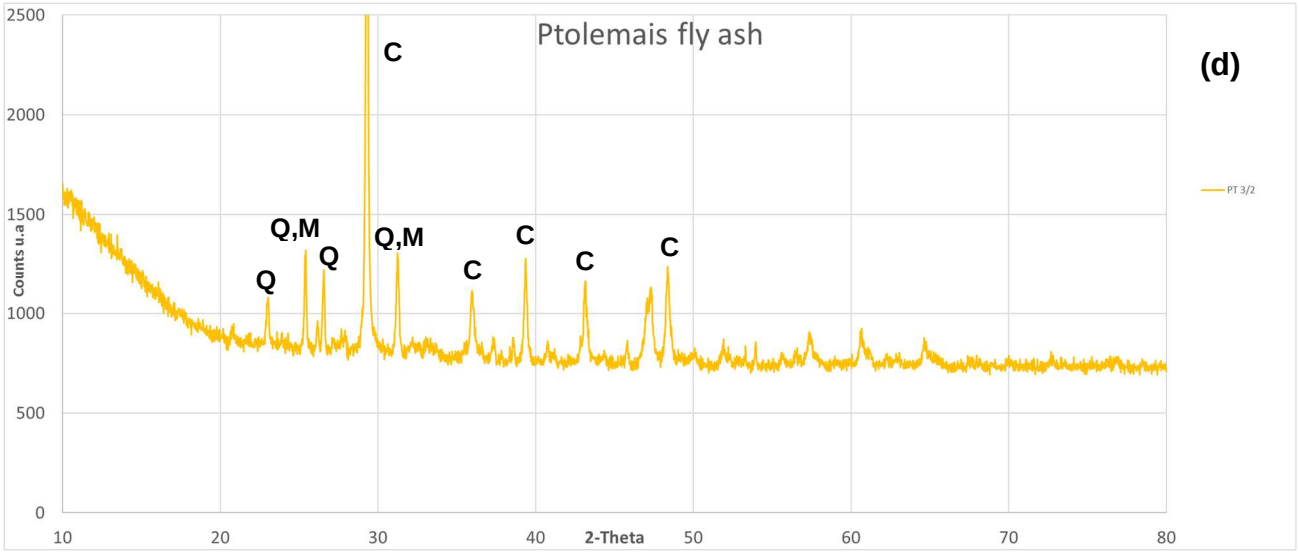

Figure 19. XRD pattern of the High-calcium fly ashes after and before carbonation (a) Before carbonation (b)After carbonation. Dry conditions.160ºC (c)After carbonation. Dry conditions. 220ºC (d) After carbonation. Wet conditions. 160ºC. Q=Quartz (SiO_2) C=Calcite ($CaCO_3$) H=Hematite (Fe_2O_3) L=Lime (CaO) M=Mullite (Al_2SiO_3)

From the XRD peaks of the high-calcium fly ashes, the mineral phases identified are calcite, mullite, lime, quartz and hematite. Figure 19 reveals an increase of calcite peaks, mainly in PT-3, and a decrease of lime peaks due to the carbonation of the fly ash. Mullite, Hematite and Quartz peaks are present in almost all the samples of the Greek fly ash, except PT/3. The positions of these peaks remain relatively constant for all the experiments.

5 Discussion

5.1 Scanning electron mapping

Scanning electron microscopy (SEM) provides high resolution images of the samples by rastering a focussed electron beam on the sample. SEM images allows to distinguish any difference between the particles that conform the sample. An energy dispersive X-ray analyser is used to identify the elemental composition of these particles and provide a quantitative compositional information. Moreover, the data of EDX is used to determine qualitatively the elemental composition of the cenospheres and analyse any significant difference between particles of the sample.

The amount of cenospheres differs between Andorra and Ptolemais fly ashes. This variation occurs due to the difference between their original mineral forms (shown in Table 6) and their thermochemical and phase transformations in the course of their combustion. (Fomenko et al., 2011)

The dark cenospheres observed with the BSD presents a higher composition of CaO, Fe_2O_3 and Al_2O_3. The light cenospheres are poor in these oxides and hence rich in SiO_2. This difference in colour is linked to the quantity of backscattered (or reflected) electrons of the electron beam, which in turn depends on the atomic mass. As the atomic mass increases, the more electrons are reflected. Of all the aforementioned elements, Quartz (SiO_2) has the highest atomic mass and hence reflects more electrons. The difference in chemical and phase-mineral compositions results in a wide diversity of morphological shape of the fly ash particles. (Fomenko et al.,2011)

For Andorra fly ashes, the formation of iron carbonate was observed on the surface of the cenospheres after carbonation. Furthermore, the samples carbonated forming isolated rhombohedral crystals and rod-shaped crystals of calcium carbonate, as shown in Figure 32.

For high calcium fly ashes, the difference before and after carbonation was clearly distinguished. The cenospheres observed after carbonation were altered and presented a series of triangular crystals on its surface that turned out to be iron carbonate. Calcium carbonate was also detected on the surface of these spherical structures, as shown in Figure 30. Some of the samples also presented isolated crystals of calcium carbonate, as shown in Figure 20.

Carbon content, visible in all samples was very high due to the presence of unburnt particles and/or the alteration of the sample due to the transmission of carbon to the sample.

The morphology of the fly ash changed after carbonation forming needle-like and rhombohedral structures (Calcite). The formation of the needle-shaped structure was only observed in samples And/3 and PT/3/2, as shown in Figure 20 and 32. This structure might correspond to aragonite and its formation might depend on the moisture content. Calcite

was observed in most of the samples and hence can be considered the main polymorph of $CaCO_3$ formed during carbonation.

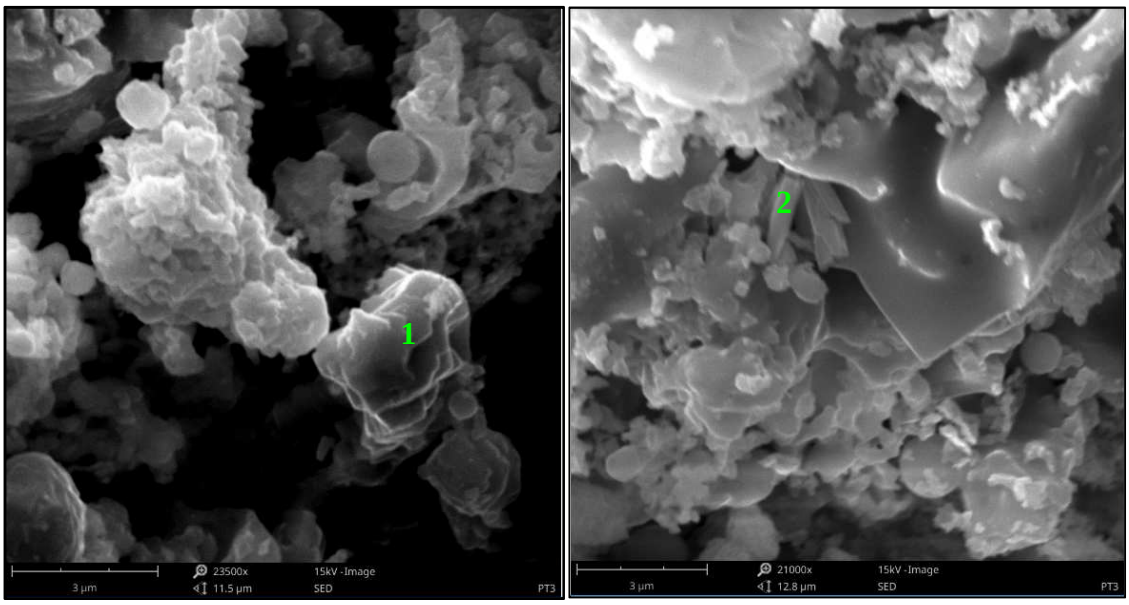

Figure 20. Rhombohedral crystal (left), which corresponds to calcite and is referenced as 1. Rod-shaped crystals (right), which might correspond to Aragonite and is referenced as 2.

5.2 X-ray diffraction

This technique is very precise when analysing minerals proportions higher than a 5%. XRD allows to identify the crystalline phases commonly observed in fly ashes.

Andorra fly ash, which has a low-calcium content, presents a relatively simple mineralogy consisting of mullite, hematite and lime. Mullite is a stable solid solution phase of alumina and silica that remains stable at atmospheric pressure. Hematite is formed during combustion when pyrite oxidizes. This mineral is quite stable as no changes are observed in the location of its peaks. Lime is present in this fly ash before carbonation and it's consumed completely after this process, as expected. Despite the decrease of lime, no carbonates were observed for any of the samples. This result reveals that the amount of calcium carbonate formed with the Andorra fly ash is imperceptible with XRD. These results also indicate that XRD under this thesis set up conditions can't quantify the changes for the Spanish fly ash after carbonation.

Lime, mullite and Hematite are also present in high-calcium fly ashes. These peaks are in similar positions as the ones observed in the Andorra Fly ash. Due to the higher content of calcium, a significant amount of lime can be observed before carbonation (only under dry conditions). This fly ash shows a consumption of lime during carbonation resulting in the formation of precipitates such as calcite.

Calcite increased in all the HCFA samples. The analysis results of the Greek fly ash show that the formation of calcite is slightly influenced by temperature and considerably affected by the moisture content. The analysis results of the Ptolemais fly ash show slight differences between the spectrums before and after carbonation under dry conditions

(PT/1 and PT/2), as both samples present similar peaks to those observed in the clean sample. However, sample PT/3/2 which was done under wet conditions registered the same peaks observed in the above-mentioned experiments (PT/1 and PT/2) and a noticeable amount of new calcite peaks. Therefore, the efficiency of the carbonation is higher under wet conditions.

Is not possible to quantify the changes of the samples after carbonation by using XRD under this thesis set up conditions. Nevertheless, it reveals mineralogical changes. Calcite is present in all the Greek fly ash samples

6 Conclusions

SEM and XRD results suggest a correlation between carbonation rate and parameters such as temperature and moisture content. Moreover, from the experiments carried out it can be deduced that the carbonation rate strongly depends on the free lime content. This compound is very reactive and tends to react with carbon dioxide to form calcite.

In this thesis, calcium oxide which is present in both samples of fly ash reacts with CO_2 under dry and wet conditions. The amount of CO_2 binded in a different form of carbonates seems to increase as the pressure increases. However, under wet conditions this amount seems to increase up to a certain pressure where the sample gets saturated with CO_2 and from there it remains constant regardless of the increase in pressure. As a result, it carbonates faster than in dry conditions (Bobicki et al., 2012; Dananjayan et al.,2015).

The results provided by SEM show the morphological variation for each sample of the cenospheres surface after and before carbonation. This method results reveals the formation of isolated crystals of calcium carbonate and an alteration of the elemental composition of the surface of the cenospheres. Further study is required in order to analyse if moisture content induces the formation of needle-like structures, which could correspond to aragonite.

XRD revealed a significant chemical transformation from lime into calcite in the Greek fly ash. On the other hand, the spectrums for Andorra Fly ash didn't show any characteristic peaks which could indicate that carbonation occurred. However, this method is very inaccurate at very low mineral changes so the results obtained with this method aren't completely reliable. Greek fly ash showed an increment of calcite peaks after carbonation, especially in PT-3. The results observed in PT/3 indicates that moisture content increases substantially the rate and efficiency of carbonation.

The results of this thesis revealed the reactivity of lignite fly ash when it's in contact with Carbon dioxide. This fly ash has a higher content of calcium oxide than bituminous and anthracite fly ashes and that is why it tends to form a higher content of precipitates of calcium carbonates when it's in contact with carbon dioxide. Calcium carbonate is a stable phase that can used to sequester CO2. and therefore, reduce the CO2 emissions caused by anthropogenic activities such as professional power industry.

Further investigations are required in order to enhance the carbonation rate with low cost energy processes. Therefore, fly ash class F should be ruled out as it doesn't have enough calcium oxide to proceed with future experiments involving carbonation of fly ashes. To enhance lignite fly ash carbonation, the CO_2 flow rate must be reduced, samples should be obtained from diverse sources in order to study the effect of potential fundamental changes of CFA properties such as the variability of the coal fly ash mineralogical properties. (Jo et al.,2012). Atomic Force Microscopy could be used to know under which conditions we have the most CO_2 capture (Demanet, 1994)

7 References

ACAA, 2007. Coal Combustion Product (CCP) Production& Use Survey Results. ACAA 15200 E. Girard Ave., Ste. 3050. Aurora, CO 80014. 9/15/2008. 1pp

Ahmaruzzaman (2010). A review on the utilization of fly ash. Prog. Energy Combust. Sci. 36 (3), Pages 327-363.

Allison et al. (2009) The Copenhagen Diagnosis: Updating the World on the Latest Climate Science. The University of New South Wales Climate Change Research Centre (CCRC), Sydney, Australia, 60pp.

Barnes & Sear (2004) Ash Utilisation from Coal-Based Power Plants. DTI Cleaner Fossil Fuels Programme.

Barnes (2010) Ash Utilisation-Impact of recent changes in power generation practices. International Energy Agency Clean Coal centre. Vol 1 page 51.

Blissett & Rowson (2012) A review of the multi-component utilisation of coal fly ash. Fuel 97, pp 1–23

Chowdhury et al. (2013). CO_2 capture with a novel solid fluidizable sorbent: thermodynamics and temperature programmed carbonation-decarbonation. Chem. Eng. J. 232, Pages 139-148.

Dananjayan et al. (2016) Direct mineral carbonation of coal fly ash for CO_2 sequestration. Journal of Cleaner Production. ISBN: 978-93-83083-87-9

Demanet (1995) Atomic force microscopy determination of the topography of fly-ash particles. Applied Surface Science 89. Pages: 97-101

Detwiler (1997) The Role of Fly Ash Composition in Reducing Alkali-Silica Reaction. Research & development information. Portland Cement association

Dubina et al. (2013). Influence of water vapour and carbon dioxide on free lime during storage at 80 ºC, studied by Raman spectroscopy. Spectrochim. Acta, Part A 111, Pages 299-303.

Egerton (2005) Physical Principles of Electron Microscopy. Springer. **ISBN-10** 0-387-25800-0. **ISBN-13** 978-0387-25800-0

Feuerborn (2011) Coal combustion products in Europe-an update on production and utilisation, standardisation and regulation. World of Coal ash conference, Denver, CO, USA. May 9-12

Feuerborn et al. (2012) Use of calcareous fly ash in Germany. Proceedings of the International conference" Eurocoalash 2012", Thessaloniki, Greece. April 11-15

Fomenko et al.(2011) Fly ash cenospheres: Composition, Morphology, Structure and Helium permeability. World of Coal Ash (WOCA) conference, Denver, USA

Friedlingstein, P. et al., (2006) Climate-carbon cycle feedback analysis: Results from the C4MIP model intercomparison. Journal of Climate 19, 3337-3353.

Ghosal & Self (1994) Particle size-density relation and cenosphere content of coal fly ash. Fuel Vol 74 No. 4, pp. 522-529

Global CCS Institute. (2015). The global Status of CCS | 2015: Summary Report. Melbourne.

Goumans et al. (1994) Environmental aspects of construction with waste material. Elsevier Science. **ISBN** 0-444-81853-7

Goumans et.al (1997) Waste Materials in Construction: Putting Theory into Practice. Elsevier Science. **ISBN** 0-444-82771-4

Heidrich et al. (2007) CCP-Waste or Resource: Breaking the regulatory paradigms. World of Coal Ash, Covington, Kentucky, USA

Helalludin et al. (2016) Main Analytical Techniques Used for Elemental Analysis in Various Matrices Tropical Journal of Pharmaceutical Research. Available on http://www.tjpr.org http://dx.doi.org/10.4314/tjpr.v15i2.29

IEA. (2013a). Global Action to Advance Carbon Capture and Storage: A focus on Industrial Applications: Annex to Tracking Clean Energy Progress 2013. Paris.

IEA. (2013b). Technology Roadmap: Carbon Capture and Storage. Paris.

IEA. (2015a). Carbon Capture and Storage: The solution for deep emissions reductions. Paris.

IEA. (2015b). Energy Technology Perspectives 2015: Executive Summary: Mobilising Innovation to Accelerate Climate Action. Paris.

IPCC (2005) Special Report on Carbon Dioxide capture and storage IPCC Contribution of Working Group III to the Intergovernmental Panel on Climate Change

IPCC (2013) Summary for Policymakers. In: Climate Change 2013: The Physical Science Basis. Contribution of Working Group I to the Fifth Assessment Report of the Intergovernmental Panel on Climate Change

IPCC. (2014). Climate Change 2014 Synthesis Report. Contribution of Working Groups I, II, III to the Fifth Assessment Report of the Intergovernmental Panel on Climate Change. Geneva.

Jaschik et al. (2016) The utilisation of fly ash in CO_2 mineral carbonation Chemical and Process Engineering. Pages 29-39

Jo et al. (2012) Evaluation of factors affecting mineral carbonation of CO_2 using coal fly ash in aqueous solutions under ambient conditions. Chemical Engineering Journal. Volume 183, 15 February 2012, Pages 77-87

Kelemen, P. B., & Matter, J. (2008). In situ carbonation of peridotite for CO 2 storage. PNAS, 105(45), 17295–17300.

Lafuente B et al. (2015). The power of databases: the RRUFF project. In: Highlights in Mineralogical Crystallography, Armbruster, T.m and Danisi, R.M., eds. Berlin, Germany, W. De Gruyter, pp 1-30

Li et al. (2005) Characterization of coal by thermal analysis methods. Thermal Analysis. Fundamentals and Applications to Material Characterization, 2005: 111-120. ISBN: 84-9749-100-9

Mazella et al. (2016) CO_2 uptake capacity of coal fly ash: Influence of pressure and temperature on direct gas-solid carbonation. Journal of Environmental Chemical Engineering

M.Cuéllar-Franca & Azapagic (2015) Carbon capture, storage and utilisation technologies: A critical analysis and comparison of their life cycle environmental impacts. Journal of CO_2 Utilization

Quorum technologies. (2008). K950X - Instruction Manual-A4407131-Issue 9. Emitech. Pages 36

Reynolds et al. (2014) Field Application of Accelerated Mineral Carbonation. Journal Minerals. Volume 4. Pages 191-207

Revathy et al. (2015) Direct Mineral Carbonation of Coal Fly Ash at Varying Low Pressure Conditions. Energy Technologies, Climate Change and Environmental Sustainability: Innovative Perspective. ISBN: 978-93-83083-87-9

Ronald et al. (2002) Chemistry of the Environment 2nd Edition. Elsevier Science & Technology Books. ISBN: 0120734613

Shaheen et al. (2014) Opportunities and challenges in the use of coal fly ash for soil improvements - A review, Journal of Environmental Management, 145, pp 249-267

Simonescu (2012). Application of FTIR Spectroscopy in Environmental Studies. "Advanced Aspects of Spectroscopy", book edited by Muhammad Akhyar Farrukh, ISBN 978-953-51-0715-6

Siriruang et al. (2016) CO_2 capture using fly ash from coal fired power plant and applications of CO_2-captured fly ash as a mineral admixture for concrete. Journal of Environmental Management 170.Pages 70-78

Skodras et al. (2005) Coal fly-ash utilisation in Greece. World of Coal ash conference, Lexington, Kentucky, USA. September 25-27

Stuart, B. H. (2004). Infrared Spectroscopy: Fundamentals and Applications. Analytical Techniques in the Sciences, Willey (Ed.), Methods (Vol. 8) pp. 224

Thomas (2007) Optimizing the Use of Fly Ash in Concrete. Portland Cement Association. IS548

Uliasz-Bocheńczyk et al. (2009) Estimation of CO_2 sequestration potential via mineral carbonation in fly ash from lignite combustion in Poland. Energy Procedia 1 4873-4879.

Uliasz-Bocheńczyk et al. (2015) Fly ash from energy production –a waste, byproduct and raw material. Volume 31. Pages 139-150

Links

https://www.perkinelmer.com/lab-solutions/resources/docs/faq_beginners-guide-to-thermogravimetric-analysis_009380c_01.pdf

https://www.lucideon.com/testing-characterization/techniques/sem-edx

https://www.c2es.org

Appendix A

PT/1

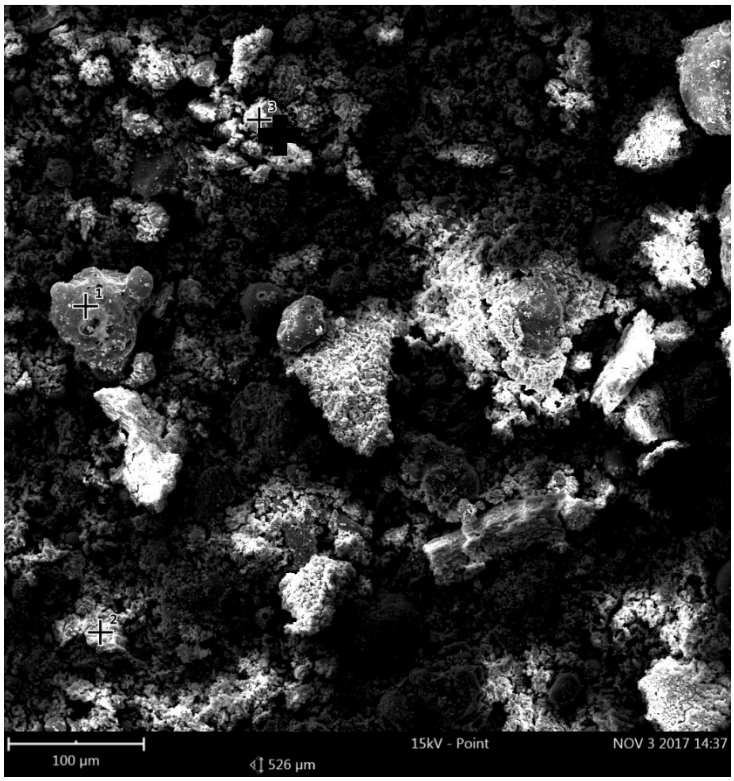

Figure 21.SEM image of Ptolemais fly ash after carbonation

Table 9. EDX quantitative analysis of element 1 from sample PT/1

1	Oxygen (O)	Silicon (Si)	Aluminium (Al)	Potassium (K)	Calcium (Ca)	Sodium (Na)
at (%)	67.39	21.14	5.34	2.46	2.11	1.10
wt (%)	52.98	29.18	7.08	4.72	4.16	1.24

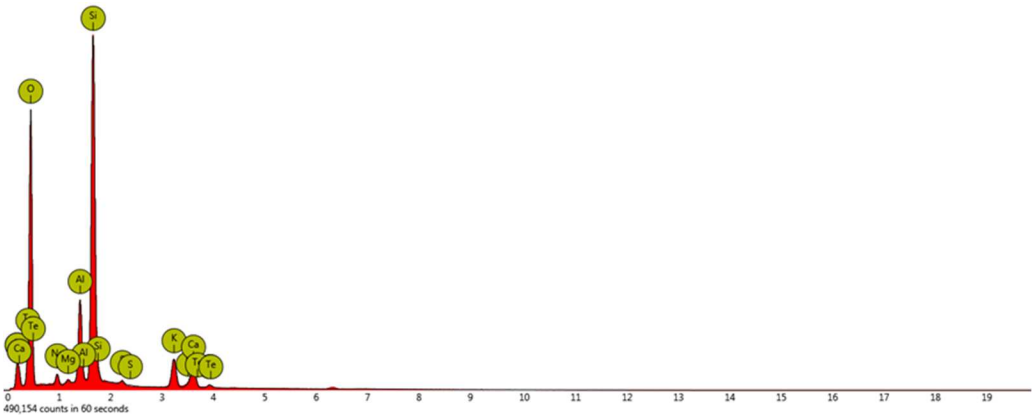

Figure 22.EDX spectrum of element 1 from sample PT/1

Table 10. EDX quantitative analysis of element 2 from sample PT/1

2	Oxygen (O)	Calcium (Ca)	Carbon (C)	Iodine (I)	Sulfur (S)	Silicon (Si)
at (%)	63.08	10.29	23.31	0.58	1.97	0.44
wt (%)	54.29	22.18	15.06	3.94	3.39	0.67

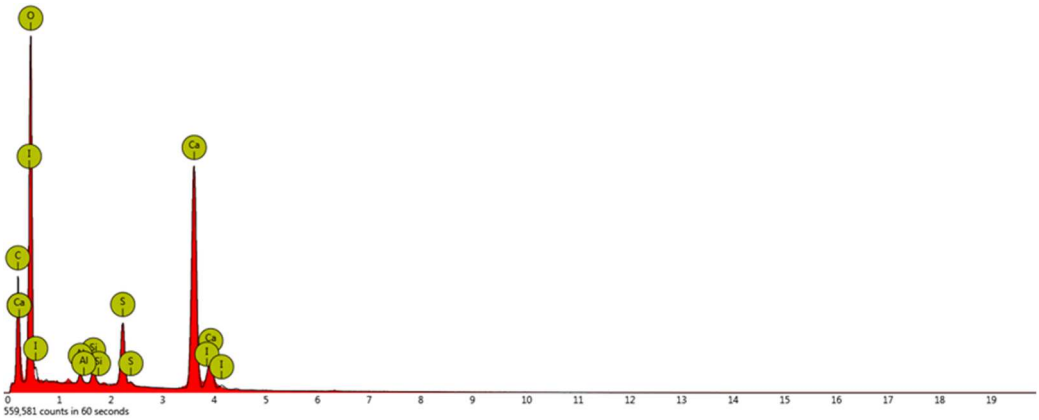

Figure 23. EDX spectrum of element 2 from sample PT/1

Table 11. EDX quantitative analysis of element 3 from sample PT/1

3	Oxygen (O)	Calcium (Ca)	Carbon (C)	Antimony (Sb)	Silicon (Si)	Iodine (I)	Sulfur (S)	Aluminium (Al)	Magnesium (Mg)
at (%)	61.09	11.45	20.82	0.63	2.09	0.42	1.18	1.37	0.94
wt (%)	49.54	23.35	12.68	3.90	2.98	2.71	1.92	1.88	1.15

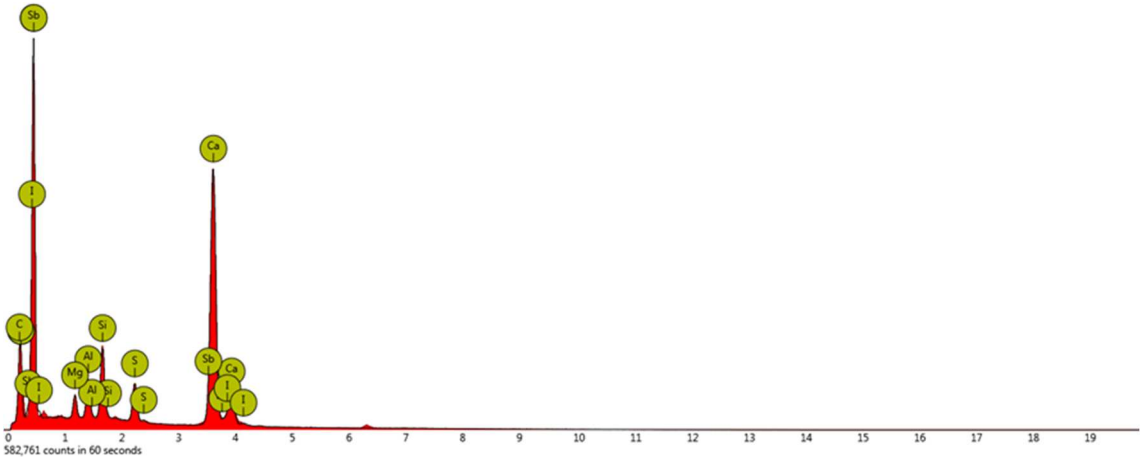

Figure 24.EDX spectrum of element 3 from sample PT/1

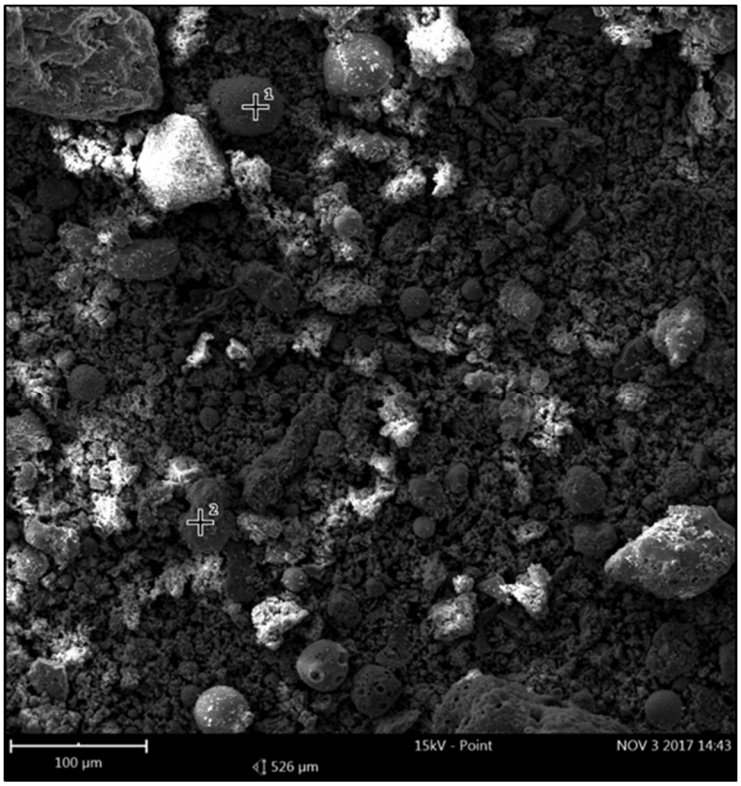

Figure 25.SEM image of the sample PT/1 after carbonation.

Table 12.EDX quantitative analysis of element 1 from sample PT/1

1	Oxygen (O)	Calcium (Ca)	Carbon (C)	Antimony (Sb)	Silicon (Si)	Iodine (I)	Sulfur (S)	Aluminium (Al)	Magnesium (Mg)	Iron (Fe)
at (%)	42.35	15.22	29.81	0.95	1.01	0.26	0.49	2.70	4.20	3.02
wt (%)	31.06	27.95	16.41	5.28	1.30	1.52	0.72	3.34	4.68	7.74

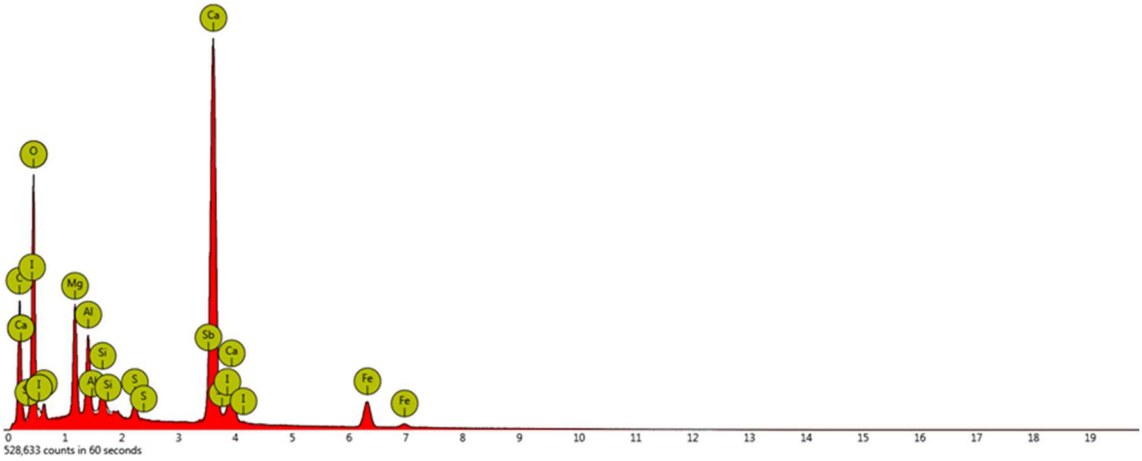

Figure 26. EDX spectrum of element 1 from sample PT/1

Table 13. EDX quantitative analysis of element 1 from sample PT/1

2	Oxygen (O)	Calcium (Ca)	Carbon (C)	Iron (Fe)	Silicon (Si)	Bromine (Br)	Magnesium (Mg)	Yttrium (Y)
at (%)	21.65	21.15	35.60	6.80	7.73	3.24	3.03	0.39
wt (%)	13.33	32.62	16.45	14.62	8.35	9.95	2.84	1.34

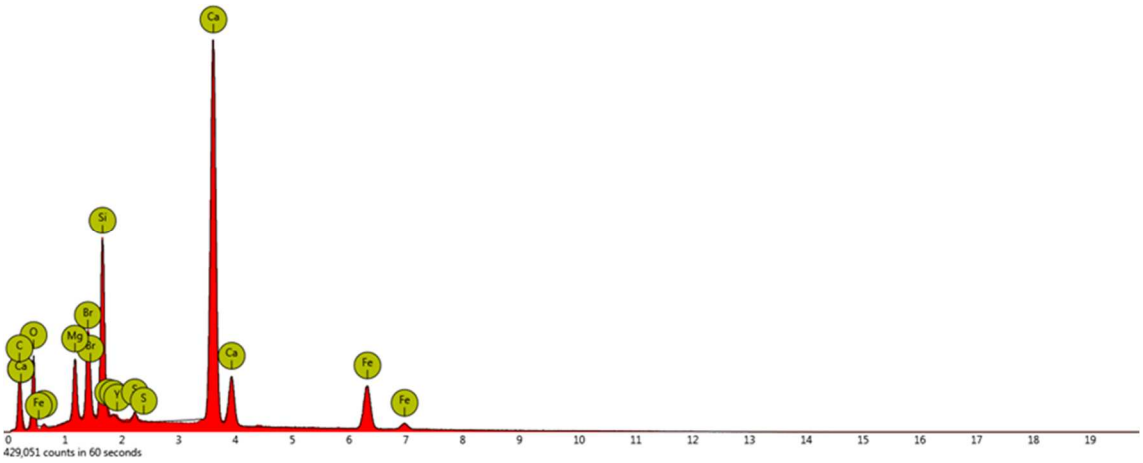

Figure 27. EDX spectrum of element 2 from sample PT/1

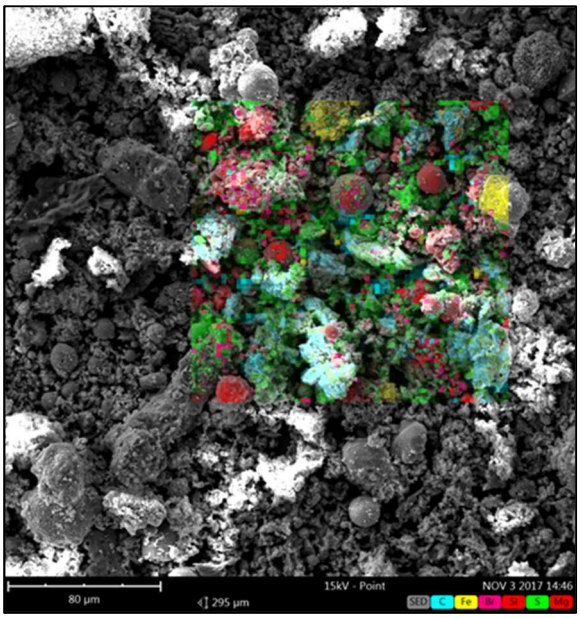

Figure 28.Mapping of the sample PT/1 after carbonation

Table 14. EDX quantitative analysis of the mapping of sample PT/1

1	Oxygen (O)	Calcium (Ca)	Carbon (C)	Iron (Fe)	Silicon (Si)	Bromine (Br)	Sulfur (S)	Magnesium (Mg)
at (%)	53.31	17.60	20.94	1.82	2.06	1.17	1.74	1.35
wt (%)	39.64	32.78	11.69	4.73	2.69	4.36	2.59	1.53

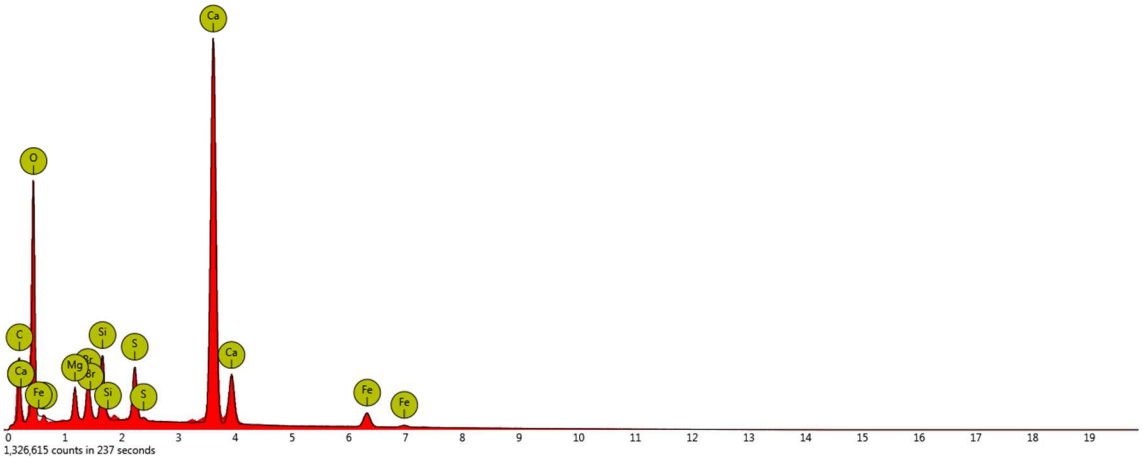

Figure 29. EDX spectrum of the mapping of sample PT/1

PT/2

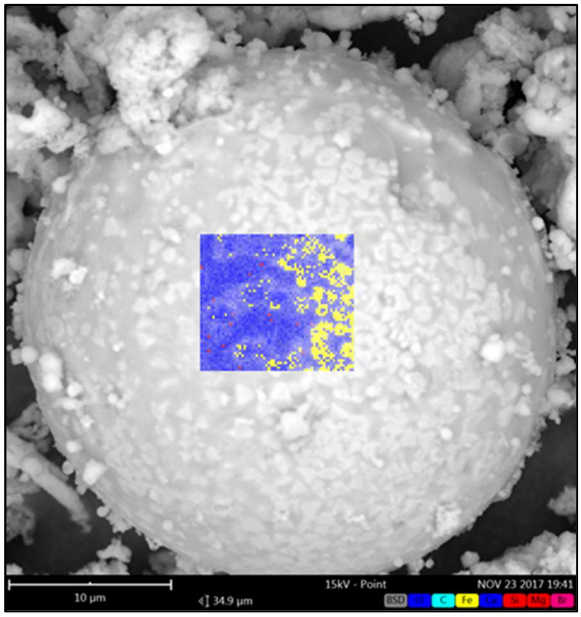

Figure 30. Mapping of the surface of a cenosphere of sample PT/2 after carbonation

Table 15. EDX quantitative analysis of the mapping of sample PT/2

1	Oxygen (O)	Calcium (Ca)	Carbon (C)	Magnesium (Mg)	Silicon (Si)	Iron (Fe)	Bromine (Br)
at (%)	48.51	9.63	19.08	3.54	6.51	9.66	3.07
wt (%)	31.74	15.79	9.38	3.52	7.48	22.08	10.02

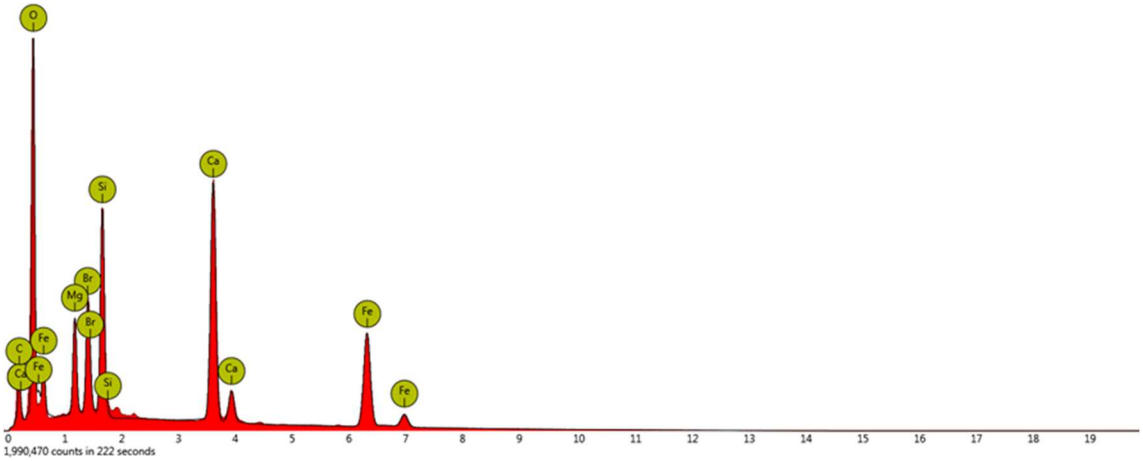

Figure 31. EDX spectrum of the mapping of sample PT/2

And /3

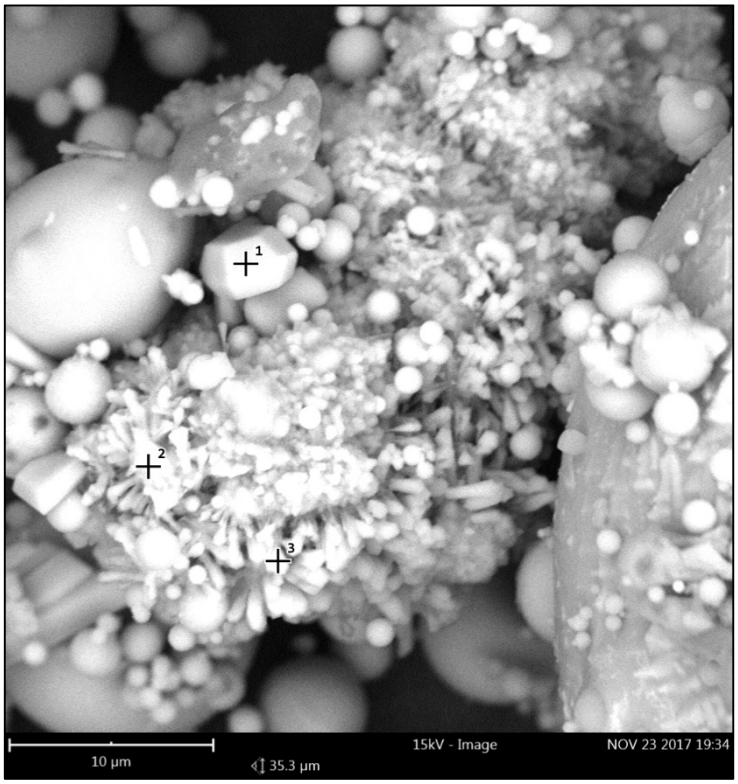

Figure 32.SEM image of the sample And/3 after carbonation.

Table 16. EDX quantitative analysis of element 1 from sample And/3

1	Oxygen (O)	Calcium (Ca)	Carbon (C)	Silicon (Si)	Sulfur (S)
at (%)	69.05	16.43	6.93	6.92	0.67
wt (%)	60.69	10.84	15.26	12.19	1.03

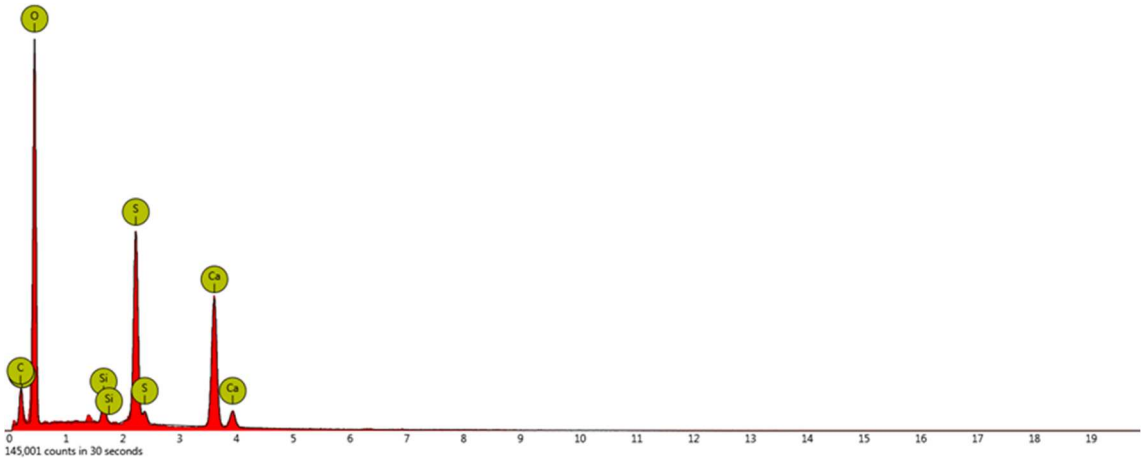

Figure 33. EDX spectrum of element 1 from sample And/3

Table 17. EDX quantitative analysis of element 2 from sample And/3

2	Oxygen (O)	Calcium (Ca)	Carbon (C)	Silicon (Si)	Sulfur (S)	Iron (Fe)	Aluminium (Al)	Magnesium (Mg)
at (%)	58.63	7.19	30.31	0.71	0.80	0.62	0.76	0.86
wt (%)	54.29	16.68	21.07	1.15	1.48	2.01	1.19	1.21

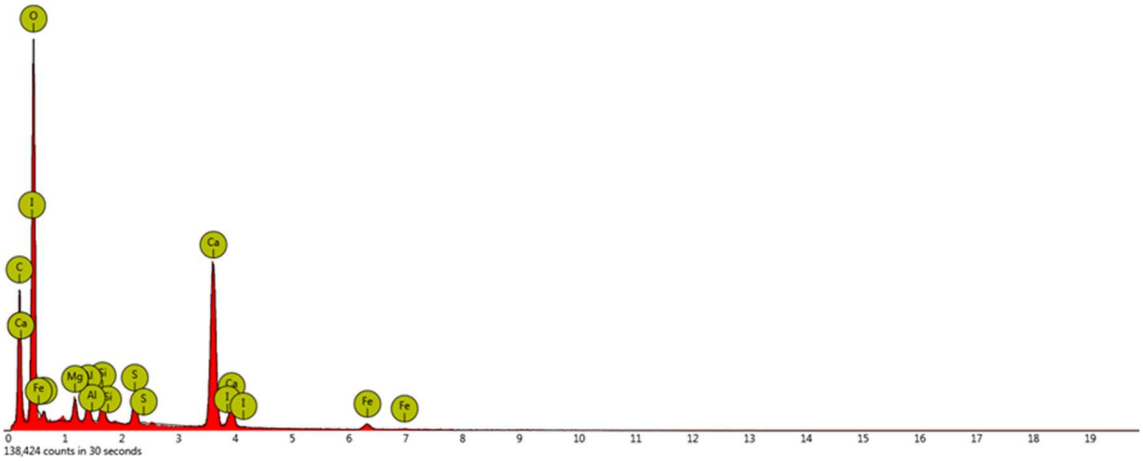

Figure 34. EDX spectrum of element 2 from sample And/3

Table 18. EDX quantitative analysis of element 3 from sample And/3

3	Oxygen (O)	Calcium (Ca)	Carbon (C)	Silicon (Si)	Aluminium (Al)
at (%)	60.75	8.11	29.51	0.56	0.52
wt (%)	56.73	18.96	20.69	0.92	0.81

Appendix B

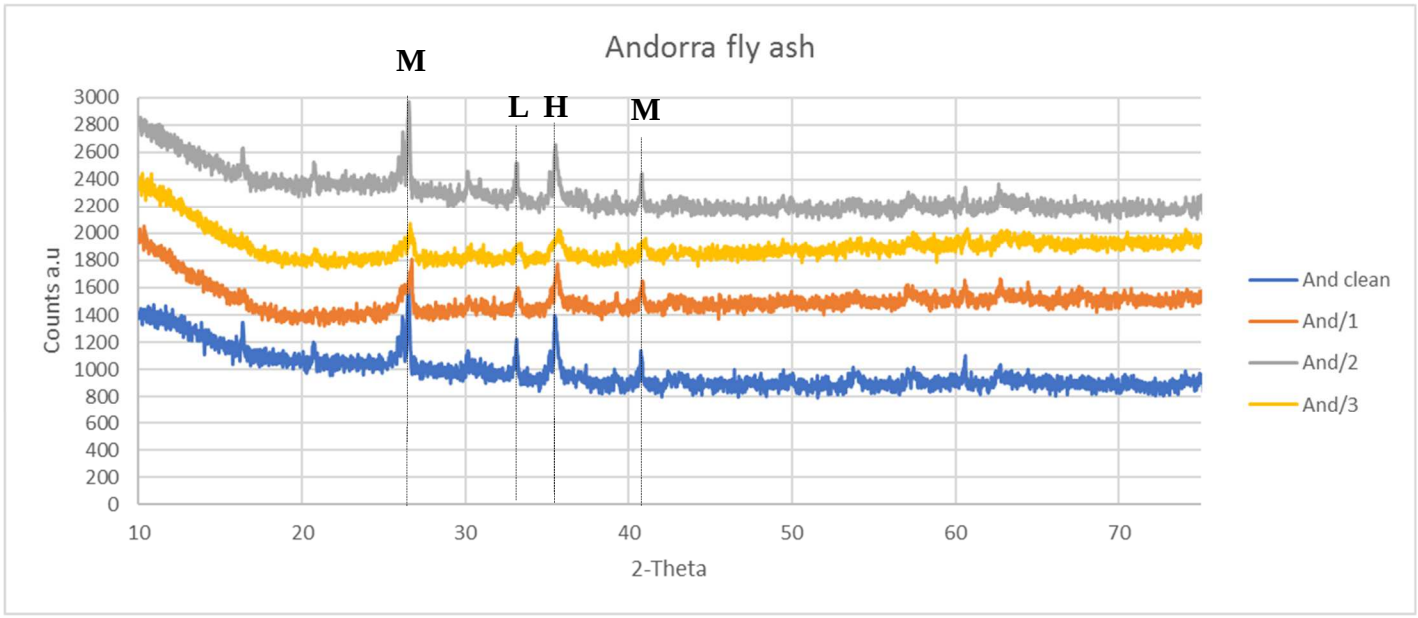

Figure 35.X-ray diffraction of the Andorra Fly ashes. M=Mullite(Al_2SiO_3) H=Hematite(Fe_2O_3) L=Lime (CaO)

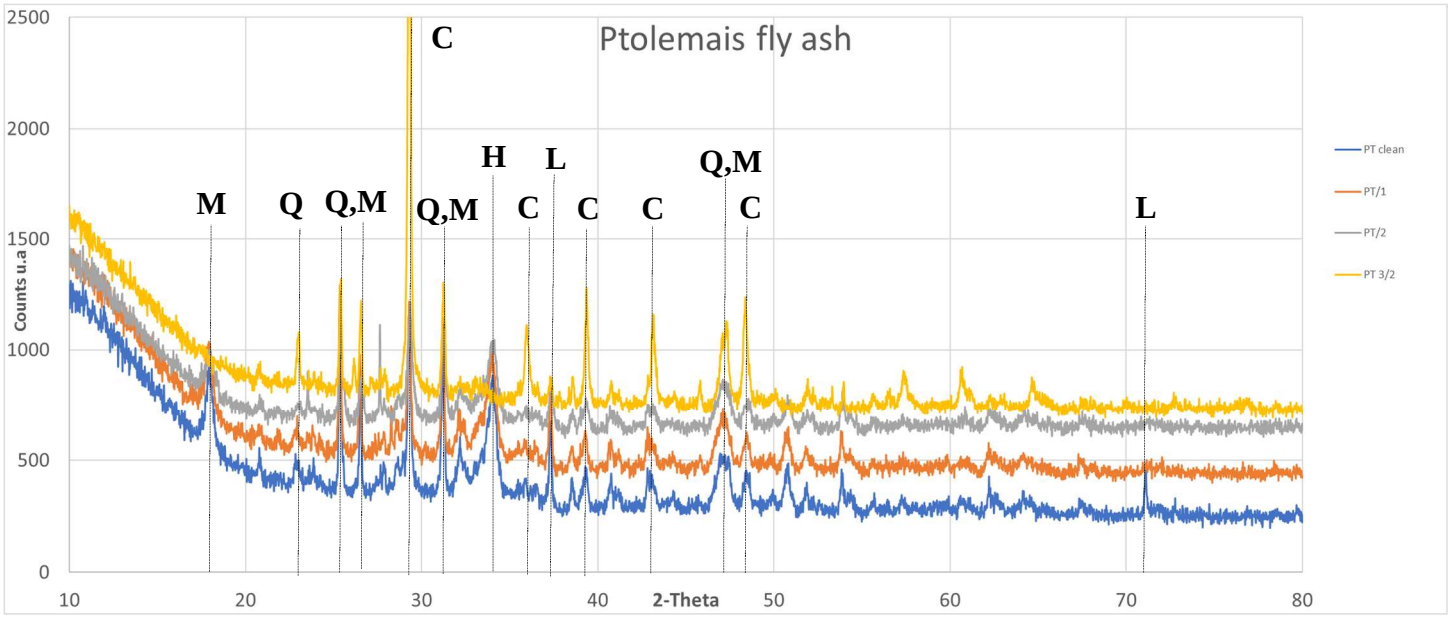

Figure 36.X-ray diffraction of the Ptolemais fly ashes. M=Mullite(Al_2SiO_3) H=Hematite(Fe_2O_3) L=Lime (CaO) C=Calcite ($CaCO_3$)